BMC Biology

Enhanced hepatic respiratory capacity and altered lipid metabolism support metabolic homeostasis during short-term hypoxic stress

--Manuscript Draft--

Manuscript Number:	BMCB-D-21-00115R4
Full Title:	Enhanced hepatic respiratory capacity and altered lipid metabolism support metabolic homeostasis during short-term hypoxic stress
Article Type:	Research article

Abstract:

Background
Tissue hypoxia is a key feature of several endemic hepatic diseases, including alcoholic and non-alcoholic fatty liver disease, and organ failure. Hypoxia imposes a severe metabolic challenge on the liver, potentially disrupting its capacity to carry out essential functions including fuel storage and the integration of lipid metabolism at the whole-body level. Mitochondrial respiratory function is understood to be critical in mediating the hepatic hypoxic response, yet the time dependent nature of this response and the role of the respiratory chain in this remain unclear.

Results
Here we report that hepatic respiratory capacity is enhanced following short-term exposure to hypoxia (2 days, 10% O_2), and is associated with increased abundance of the respiratory chain supercomplex III_2+IV and increased cardiolipin levels. Suppression of this enhanced respiratory capacity, achieved via mild inhibition of mitochondrial complex III, disrupted metabolic homeostasis. Hypoxic exposure for 2 days led to accumulation of plasma and hepatic long chain acyl-carnitines. This was observed alongside depletion of hepatic triacylglycerol species with total chain lengths of 39-53 carbons, containing palmitic, palmitoleic, stearic and oleic acids, which are associated with *de novo* lipogenesis. The changes to hepatic respiratory capacity and lipid metabolism following 2 days hypoxic exposure were transient, becoming resolved after 14 days in line with systemic acclimation to hypoxia and elevated circulating haemoglobin concentrations.

Conclusions
The liver maintains metabolic homeostasis in response to shorter term hypoxic exposure through transient enhancement of respiratory chain capacity, and alterations to lipid metabolism. These findings may have implications in understanding and treating hepatic pathologies associated with hypoxia.

Corresponding Author:	Katie Alice O'Brien University of Cambridge Cambridge, Select if applicable UNITED KINGDOM
Corresponding Author Secondary Information:	
Corresponding Author's Institution:	University of Cambridge
Corresponding Author's Secondary Institution:	
First Author:	Katie Alice O'Brien
First Author Secondary Information:	
Order of Authors:	Katie Alice O'Brien

	Ben D McNally
	Alice P Sowton
	Antonio Murgia
	James Armitage
	Luke W Thomas
	Fynn N Krause
	Lucas A Maddalena
	Ian Francis
	Stefan Kavanagh
	Dominic P Williams
	Margaret Ashcroft
	Julian L Griffin
	Jonathan J Lyon
	Andrew J Murray

Order of Authors Secondary Information:	
Response to Reviewers:	The Change of Authorship form and confirmation from all authors have been sent via email. The raw mass spectrometry data has been deposited to the EMBL-EBI MetaboLights database with the identifier MTBLS3713. This information has been included in the 'Availability of Data' section of the manuscript.

Additional Information:	
Question	**Response**
Has this manuscript been submitted before to this journal or another journal in the <a href="https://www.biomedcentral.com/p/the-bmc-series-journals#journallist" target="_blank" >BMC series</ a>?	No
Experimental design and statistics Full details of the experimental design and statistical methods used should be given in the Methods section, as detailed in our Minimum Standards Reporting Checklist. Information essential to interpreting the data presented should be made available in the figure legends. Have you included all the information requested in your manuscript?	Yes
Resources A description of all resources used, including antibodies, cell lines, animals	Yes

and software tools, with enough information to allow them to be uniquely identified, should be included in the Methods section. Authors are strongly encouraged to cite Research Resource Identifiers (RRIDs) for antibodies, model organisms and tools, where possible.

Have you included the information requested as detailed in our Minimum Standards Reporting Checklist?

1   # Enhanced hepatic respiratory capacity and altered lipid

2   # metabolism support metabolic homeostasis during short-term

3   # hypoxic stress

4   Katie A O'Brien[1]*, Ben D McNally[2], Alice P Sowton[1], Antonio Murgia[2], James Armitage[3], Luke W

5   Thomas[4], Fynn N Krause[2], Lucas A Maddalena[4], Ian Francis[5], Stefan Kavanagh[6], Dominic P Williams[7],

6   Margaret Ashcroft[4], Julian L Griffin[2,8], Jonathan J Lyon[3], Andrew J Murray[1]*.

7   [1]Department of Physiology, Development and Neuroscience, University of Cambridge, Downing Street,

8   Cambridge, CB2 3EG, UK.

9   [2]Department of Biochemistry and Cambridge Systems Biology Centre, University of Cambridge, Sanger Building

10   Tennis Court Road, Cambridge, CB2 1GA, UK.

11   [3]Global Investigative Safety, GlaxoSmithKline R&D, Park Road, Ware, Hertfordshire, SG12 0DP, UK.

12   [4]Department of Medicine, University of Cambridge, Cambridge Biomedical Campus, Hills Road, Cambridge, CB2

13   0QQ, UK.

14   [5]Ultrastructure and Cellular Bioimaging, GlaxoSmithKline R&D, Park Road, Ware, Hertfordshire, SG12 0DP, UK.

15   [6]Oncology Safety Sciences, Clinical Pharmacology & Safety Sciences, R&D, AstraZeneca, Cambridge, CB2 OAA,

16   UK.

17   [7]Functional and Mechanistic Safety, Clinical Pharmacology & Safety Sciences, R&D, AstraZeneca, Cambridge, CB2

18   OAA, UK.

19   [8]Section of Biomolecular Medicine, Department of Digestion, Metabolism and Reproduction, Imperial College

20   London, South Kensington Campus, London, SW7 2AZ, UK.

21   *Corresponding authors:

22   KA O'Brien ko337@cam.ac.uk

23   AJ Murray ajm267@cam.ac.uk

<u>Abstract</u>

Background

Tissue hypoxia is a key feature of several endemic hepatic diseases, including alcoholic and non-alcoholic fatty liver disease, and organ failure. Hypoxia imposes a severe metabolic challenge on the liver, potentially disrupting its capacity to carry out essential functions including fuel storage and the integration of lipid metabolism at the whole-body level. Mitochondrial respiratory function is understood to be critical in mediating the hepatic hypoxic response, yet the time dependent nature of this response and the role of the respiratory chain in this remain unclear.

Results

Here we report that hepatic respiratory capacity is enhanced following short-term exposure to hypoxia (2 days, 10% O_2), and is associated with increased abundance of the respiratory chain supercomplex III_2+IV and increased cardiolipin levels. Suppression of this enhanced respiratory capacity, achieved via mild inhibition of mitochondrial complex III, disrupted metabolic homeostasis. Hypoxic exposure for 2 days led to accumulation of plasma and hepatic long chain acyl-carnitines. This was observed alongside depletion of hepatic triacylglycerol species with total chain lengths of 39-53 carbons, containing palmitic, palmitoleic, stearic and oleic acids, which are associated with *de novo* lipogenesis. The changes to hepatic respiratory capacity and lipid metabolism following 2 days hypoxic exposure were transient, becoming resolved after 14 days in line with systemic acclimation to hypoxia and elevated circulating haemoglobin concentrations.

Conclusions

The liver maintains metabolic homeostasis in response to shorter term hypoxic exposure through transient enhancement of respiratory chain capacity, and alterations to lipid metabolism. These findings may have implications in understanding and treating hepatic pathologies associated with hypoxia.

2

Background

51   Tissue hypoxia can arise as a result of disrupted convective oxygen (O_2) delivery, and imposes an

52   energetic challenge on the tissues (1). The liver plays a key role in integrating fuel storage and systemic

53   metabolism, in particular lipid metabolism, and requires significant O_2 to perform this role. This results

54   in steep O_2 gradients across liver lobules and a high susceptibility to hypoxia (2). Hepatic hypoxia is a

55   key feature of a number of medical conditions and has been implicated in the development of both

56   alcoholic and non-alcoholic fatty liver disease (2).

57   It has been suggested that alterations in respiratory function play a key role in linking tissue hypoxia,

58   oxidative stress and lipid metabolism in the liver, with the role of the mitochondria having been

59   identified as a specific knowledge gap in current understanding of pathological hepatic hypoxia (3).

60   The key molecular mediators of the cellular hypoxia response are the hypoxia inducible factor (HIF)

61   family of transcription factors and associated regulatory proteins (4, 5). Reactive oxygen species

62   production by mitochondrial complex I (CI) and III (CIII) can mediate activation of HIF1α and HIF2α, an

63   effect demonstrated within minutes of hypoxic exposure across a range of cell types (6-9).

64   Mitochondrial oxidative capacity is rapidly targeted in hypoxia, with Na^+ entry via the mitochondrial

65   Na^+/Ca^{2+} exchanger decreasing the mobility of free ubiquinone, and in doing so impairing electron

66   transfer to CIII (10). The electron transfer system (ETS), and particularly signalling via CIII, is therefore

67   integral to the metabolic response to hypoxic exposure.

68   HIF activation is associated with alterations in metabolism and mitochondrial O_2 consumption (11) in

69   both cells (12, 13) and tissues including heart (14) and skeletal muscle (15, 16). In the heart, HIF

70   activation has been associated with the suppression of fatty acid oxidation mediated via

71   downregulation of peroxisome proliferator-activated receptor α (PPARα) (14). In skeletal muscle,

3

72 constitutive HIF activation has been linked to increased reliance on glycolytic ATP production (15, 16)

73 and suppression of mitochondrial respiratory capacity (16).

74 In the liver, the activation of HIF1α and HIF2α are associated with contrasting effects. HIF2α is

75 purported to stimulate lipogenesis and inhibit fatty acid oxidation (17), whereas it has been suggested

76 that HIF1α prevents excess lipid accumulation in fatty liver by suppressing the sterol response element

77 binding protein (SREBP)-1c-dependent lipogenic pathway (18). Through the use of HIF1α-null mice,

78 HIF1α activity has been linked to suppression of PPARα in liver and consequential downregulation of

79 its transcriptional targets, including carnitine palmitoyltransferase 1 (CPT1) (18). However, this

80 contrasts with reports of increased hepatic PPARα and CPT1 expression in rats following 3 days of

81 hypoxic exposure (19). These apparent contradictions may reflect time-dependent aspects of the HIF

82 response. Indeed, it has been posited that HIF1α underpins the response to more acute (<24 h)

83 exposure whilst HIF2α coordinates longer-term changes in response to more sustained hypoxia (20).

84 Elucidating the time-dependent nature of the hepatic metabolic response to hypoxia is therefore an

85 important area of investigation.

86 Here we investigated the metabolic response of rat liver to short-term (2 days) and prolonged (14

87 days) exposure to inhalation hypoxia (10% O_2). The role of the mitochondrial ETS in this response, and

88 so the importance of altered respiratory capacity, was probed through the mild inhibition of CIII (21).

89 To assess the consequences for hepatic and systemic metabolic regulation, metabolomic profiles were

90 examined in liver and plasma, with a particular focus on alterations in lipid metabolism.

91 We demonstrate that maintenance of hepatic metabolic homeostasis during short term hypoxic

92 exposure is dependent on enhanced respiratory capacity, a response associated with mitochondrial

93 respiratory supercomplex formation. Notably, this effect was transient, with respiratory capacity

94 returning to normoxic levels after 14 days exposure. Lipid homeostasis was substantially altered after

95 2 days of hypoxic exposure and this was partially dependent on alterations in respiratory capacity.

96

4

97   **Results**

98   **Hepatic mitochondrial response to shorter-term and more sustained hypoxic exposure and the role**

99   **of the electron transfer system**

100   Female Crl:CD(SD) rats (220-300 g, n = 8-10/group) were exposed to normoxia or hypoxia (10% O_2) for

101   either 2 days or 14 days. The degree and duration of hypoxic exposure were based upon prior work

102   demonstrating time dependent effects of 10% O_2 exposure on respiratory capacity in rat heart and

103   skeletal muscle (22). Following hypoxic exposure, a mitochondrial CIII inhibitor (GSK932121A, 25 mg

104   kg^{-1}) or vehicle (Veh) was administered *i.p.* (**Figure 1A**, see Methods). GSK932121A binds to the Qi site

105   of CIII (23) and inhibits CIII catalytic activity in rodents (21) Prior work has demonstrated its toxic

106   effects upon mitochondrial function in female Crl:CD(SD) rats when administered at a dose of 50 mg

107   kg^{-1} *i.p.* (21) . The dose used here is below that shown to invoke overt hepatotoxicity, with the aim

108   being to exert mild CIII inhibition.

109   Sustained exposure to hypoxia induced an expected systemic response, including 27% higher blood

110   haemoglobin concentrations ([Hb]) after 14 days compared with that of normoxic rats (p < 0.0001)

111   (**Figure 1B**). No rise in [Hb] was observed after 2 days of hypoxia, indicating that systemic acclimation

112   to hypoxia had not occurred at this timepoint. Following GSK932121A or Veh administration, animals

113   were euthanised after 1.5-3.5 h, based on the severity of clinical signs (ventilation rate, piloerection,

114   hunched posture, orbital tightening and subdued behaviour (24)). Following 2 days of hypoxia,

115   GSK932121A administration resulted in increased clinical signs compared with those seen in Veh-

116   treated rats (p = 0.0002), a response that was greater than that seen in rats administered with

117   GSK932121A after 14 days of hypoxia (p = 0.03) (**Additional File 1: Figure S1A**). At termination, levels

118   of GSK932121A present in both liver and plasma did not differ between normoxic or hypoxic groups,

119   suggesting metabolism of the drug was not impacted by hypoxic exposure (**Additional File 1: Figure**

120   **S1B,C**). Following 2 days of hypoxia, GSK932121A administration resulted in 36% higher levels of liver

121   hydroxyproline compared with that seen in Veh-treated hypoxic rats (p = 0.0003) (**Additional File 1:**

5

122 **Figure S1D**), suggestive of the onset of hepatic fibrogenesis (25, 26). There was, however, no increase

123 in hepatic hydroxyproline when GSK932121A was administered to rats following 14 days of hypoxia.

124 Liver fibrosis associated with mitochondrial dysfunction has been shown to coincide with raised

125 circulating lactate (27-29), however, no rise in plasma lactate was observed here following hypoxic

126 exposure or GSK932121A administration, either alone or in combination (**Additional File 1: Figure**

127 **S1E**). Administration of GSK932121A at 50 mg kg^{-1} has been associated with hepatic glycogen

128 depletion (21), yet no change in hepatic glycogen storage was observed (**Additional File 1: Figure S1F**).

129 Together, this suggests that whilst 2 days of hypoxic exposure in combination with GSK932121A

130 administration invoked hepatic stress, the dose used did not result in overt hepatotoxicity.

131 To probe the response of hepatic mitochondria to hypoxia, we measured respiratory capacity in liver

132 homogenates using high-resolution respirometry and a substrate-uncoupler-inhibitor titration (see

133 Methods). Hepatic leak state respiration (supported by malate and octanoyl-carnitine, OctM$_L$) was not

134 altered by hypoxic exposure of either duration (**Figure 1C**). Following 2 days of hypoxia, however, both

135 hepatic fatty acid oxidation capacity (supported by malate and octanoyl-carnitine in the presence of

136 ADP, OctM$_P$, **Figure 1D**) and respiration through the N-pathway via complex I (supported by malate

137 and glutamate in the presence of ADP, GM$_P$, **Figure 1E**) showed non-significant trends towards higher

138 rates of respiration than those in normoxic rats (p = 0.08). Maximal oxidative phosphorylation

139 (OXPHOS) capacity (supported by malate, glutamate, succinate and ADP, GMS$_P$) (**Figure 1F**) and ETS

140 capacity (supported by malate, glutamate and succinate, ADP and the uncoupler FCCP, GMS$_E$) (**Figure**

141 **1G**) were both 58% higher in the livers of rats following 2 days of hypoxic exposure compared with

142 normoxic rats (p < 0.05). This rise in hepatic respiratory capacity observed in 2 day hypoxia-exposed

143 rats was sensitive to CIII inhibition, with GSK932121A-treatment eliminating the increased maximal

144 OXPHOS capacity and ETS capacity compared with normoxic rats. Respiration through the S-pathway

145 via complex II (CII), supported by succinate in the presence of rotenone (S$_E$), was 40% higher in rats

146 following 2 days of hypoxia compared with normoxic rats (p = 0.03) (**Figure 1H**). Unlike the alterations

147 in maximal OXPHOS and ETS capacities with shorter-term hypoxia, this increase in succinate-

6

148 supported respiration was not sensitive to mild CIII inhibition with GSK932121A, suggesting that CIII

149 was not saturated in this respiratory state. No alterations to hepatic mitochondrial respiratory

150 capacity were sustained following 14 days of hypoxia, with respiration rates at this timepoint no

151 different to those in the livers of normoxic rats.

152 To understand whether the enhanced hepatic respiratory capacity following 2 days of hypoxic

153 exposure resulted from changes in liver mitochondrial content, the mitochondrial network was

154 visualised using electron microscopy (**Figure 1I**). No changes in mitochondrial number per area were

155 observed in response to either 2 days or 14 days of hypoxic exposure (**Figure 1J**). We also assessed

156 citrate synthase activity, a putative marker of mitochondrial density (30) (**Figure 1K**) and again found

157 no change following hypoxic exposure at either timepoint. This suggests that the enhanced hepatic

158 respiratory capacity observed in response to shorter-term hypoxia was not due to increased liver

159 mitochondrial content.

160 At the onset of hypoxic exposure, *ad libitum* food intake decreased in rats by 55% during day 1 and by

161 43% during day 2, compared with pre-exposure intake (**Additional File 1: Figure S2A**). This

162 corresponded to a 9.2% drop in body weight, which was recovered over subsequent days to 0.4%

163 above baseline level by day 14 (**Additional File 1: Figure S2B**). To discern the effects of decreased food

164 intake upon metabolic function over this 2 day period, female Crl:CD(SD) rats (220-300g) were single-

165 housed in normoxia for 2 days with food availability either matched to that consumed by hypoxic rats

166 or freely available as controls (n=6/group). In comparison to *ad libitum*-fed controls, pair-feeding rats

167 to match the food intake of 2 day hypoxic animals induced a 27% rise in fatty acid oxidation-supported

168 OXPHOS (p = 0.05) indicative of a fasted state. This was alongside a 23% rise in maximal ETS (p = 0.04).

169 However, there was no alteration in maximal OXPHOS capacity (**Additional File 1: Figure S2C**),

170 indicating that the rise in maximal OXPHOS capacity seen in hypoxic rats did not occur as a result of

171 lower calorie intake.

172 **Respiratory complexes and supercomplexes following short-term hypoxia**

7

173 In order to probe further mechanisms that might underpin the hepatic mitochondrial response to

174 hypoxia, we sought to investigate the formation of mitochondrial supercomplexes and the expression

175 of representative subunits of the ETS complexes. Hepatic respiratory supercomplexes were assessed

176 through blue native polyacrylamide gel electrophoresis (BN-PAGE) on mitochondrial extracts

177 solubilised using digitonin (31). Band identification was achieved through immunoblotting (**Figure 2A**

178 **and Additional File 1: Figure S3A**) and comparison to recent characterisation of supercomplex

179 structure (31, 32). Analysis was performed using gels stained with Colloidal Blue (**Figure 2B**).

180 Following 2 days of hypoxic exposure, the abundance of supercomplexes of the stoichiometric

181 combinations I+III$_2$ and III$_2$+IV co-migrated with complex V (CV) were increased by 28% (p = 0.057) and

182 35% (p = 0.0002) respectively across Veh and GSK932121A-treated groups (**Figures 2C, D**). Compared

183 with normoxia, complex I (CI) monomer abundance showed a non-significant trend towards

184 increasing, whilst complex IV (CIV) monomer abundance was 39% higher (p = 0.0005) following 2 d

185 hypoxia (**Figures 2E, F**). In response to pair-feeding, no significant change in supercomplex levels or

186 monomer abundances were observed, although a non-significant trend towards increased abundance

187 of CIV monomer of 18% (p = 0.052) was seen (**Additional File 1: Figure S3B,C**).

188 To assess whether band density changes were due to increased protein expression, the levels of

189 representative subunits of Complexes I-V were examined using immunoblotting. No statistical

190 differences were seen in protein expression of any representative subunit following hypoxic exposure

191 (**Additional File 1: Figure S4A**). This suggests the increase in band density observed for III$_2$+IV co-

192 migrated with CV was due to III$_2$+IV formation rather than increased complex V expression.

193 Supercomplex assembly requires the phospholipid cardolipin (33), synthesised on the inner

194 mitochondrial membrane (34, 35). The association of cardiolipin with the inner mitochondrial

195 membrane is dependent on double bond composition, with the C18:2–C18:2 configuration being the

196 principal species found in rat liver (36). Following 2 days of hypoxic exposure, we found cardiolipin

197 (C18:2)$_4$ levels were 38% higher compared with those in Veh-treated normoxic rats and 44% higher in

198 comparison with Veh-treated 14 day hypoxic rats (p <0.05) (**Figure 2G**). A structural component of

199 supercomplexes that bridges complexes III and IV is COX7A2L/SCAF1 (37). The expression of *Cox7a2l*

200 examined by RT-qPCR revealed a trend towards increased expression following 2 days of hypoxia (p =

201 0.06), across both Veh and GSK932121A treated animals (**Figure 2H**).

202 The assembly and stability of large supercomplexes is dependent on mitochondrial cristae shape (38)

203 regulated through oligomerisation of the inner membrane optic atrophy 1 (OPA1) (39). We therefore

204 investigated factors known to be associated with OPA1 stability, including hypoxia-induced gene

205 domain protein-1a (HIGD1A) (40), the mitochondrial solute carrier (SLC25A1) (39) and mitochondrial-

206 localised protein stomatin-like protein 2 (STOML2) (41). Hepatic expression of *Higd1a* increased by

207 62% following 2 days of hypoxia (p = 0.002), and this remained 55% higher following 14 days of hypoxia

208 (p = 0.005) (**Additional File 1: Figure S4B**). In contrast, expression of *Slc25a11* and *Stoml2* did not

209 change in response to hypoxic exposure (**Additional File 1: Figure S4C,D**).

210 Together, this implies that the enhanced hepatic mitochondrial respiratory capacity in response to 2

211 days of hypoxia exposure occurs via increased respiratory supercomplex formation and complex IV

212 monomer abundance, accompanied by elevated levels of hepatic cardiolipin, *Cox7a2l* and *Higd1a*.

213 Whilst mild inhibition of CIII suppressed respiratory function at 2 days of hypoxia, our results indicate

214 that this inhibitor did not impact supercomplex formation.

215 **The mitochondrial response to short-term hypoxia is critical for hepatic metabolic homeostasis.**

216 To investigate the importance of the hepatic mitochondrial response to hypoxia for metabolic

217 homeostasis, we employed targeted metabolomics of snap-frozen liver tissue to assess metabolites

218 critical to glycolysis, tricarboxylic acid (TCA) cycle function and energy metabolism, including

219 adenosine, guanosine and uridine phosphates alongside creatine and phosphocreatine. Remarkably,

220 levels of these metabolites were largely unaltered in rat liver following 2 days of hypoxic exposure,

221 highlighting a robust hepatic response to maintain metabolic homeostasis in the face of hypoxia

222 (**Figure 3**).

9

223 HIF pathway activation in hypoxia is known to increase expression of glycolytic enzymes (15, 16, 42),

224 whilst viability of cultured hepatocytes in acute hypoxia is dependent on glycolysis (43). Surprisingly,

225 hepatic expression of the glycolytic gene transcripts *Hk1*, *Pfk* or *Ldha* were unaltered at 2 days or 14

226 days of hypoxic exposure (**Additional File 1: Figure S5A-C**), whilst expression of *Pgk1*, encoding

227 phosphoglycerate kinase, was decreased by 55% following 2 days of hypoxia and by 49% after 14 days

228 compared to normoxia (p > 0.05) (**Additional File 1: Figure S5D**). Along with the findings that glycolytic

229 intermediates (**Figure 3**) and glycogen storage (**Additional File 1: Figure S1F**) were unaltered at 2 d

230 hypoxia, this suggests that the hepatic response to short-term hypoxic stress does not depend upon

231 increased glycolytic capacity or flux.

232 Inhibition of CIII revealed the critical role of the hepatic mitochondrial response in maintaining

233 energetic homeostasis, since GSK932121A administration to rats following 2 days of hypoxia (but not

234 normoxic rats, nor rats following 14 days of hypoxia) resulted in widespread disruption of metabolic

235 homeostasis. This was demonstrated through increased abundance of metabolites related to

236 glycolysis, suggesting that inhibition of the enhanced respiratory capacity increases glycolytic flux.

237 Moreover, the abundance of TCA cycle intermediates and metabolites related to energetic

238 homeostasis were also altered following GSK932121A-treatment after 2 days of hypoxia (p < 0.05)

239 (**Figure 3**). This indicates that the enhanced hepatic respiratory capacity seen in response to short-

240 term hypoxic stress is essential for the maintenance of metabolic homeostasis.

241 **Hepatic and systemic lipid metabolism is altered following 2 days of hypoxia**

242 Next we sought to investigate the effect of hypoxic exposure and the hepatic mitochondrial response

243 to hypoxia on lipid metabolism, beginning with examination of fatty acid derived acyl-carnitines. Total

244 plasma acyl-carnitines, including those with carbon chain lengths 2-20 (C2-20) and free/-L carnitine,

245 were 33% higher following 2 days of hypoxia in comparison with the plasma of normoxic rats (p =

246 0.007). Notably, this was the case in both Veh-treated rats and those administered GSK932121A

247 (**Figure 4A**). Following 2 days of hypoxia, hepatic levels of short chain acyl-carnitines (C5,C8), were

10

248 78% lower (p = 0.003), whilst medium and long chain acyl-carnitines (C14-C20) were 47% higher than

249 those in livers of normoxic animals (p = 0.006) (**Figure 4B**). Again, this was unaffected by GSK932121A

250 administration, suggesting that this occurs independently of the enhanced respiratory capacity seen

251 at this timepoint.

252 To further examine alterations in hepatic lipid metabolism following short-term hypoxic exposure, the

253 hepatic lipidome was analysed in an open profile manner to compare Veh-treated normoxic and 2 day

254 hypoxic rats. An orthogonal partial least squares-discriminant analysis (OPLS-DA) model readily

255 separated these groups (R^2X(cum) = 40.9%; Q^2(cum) = 69.7%), **Figure 5A**), and the model passed cross-

256 validation by random permutation (**Figure 5B,** y-axis intercepts R^2 = 0.0, 0.76; Q^2 = 0.0, -0.45) and by

257 CV-ANOVA (p = 0.004)). An S-plot was constructed and those lipid species lying 2 standard deviations

258 from the mean defined as those driving the model separation (**Figure 5C**). From this, triacylglycerols

259 (TAGs) emerged as key discriminants. Subsequent analysis therefore focused upon TAGs and revealed

260 that following 2 days of hypoxia, TAGs with carbon chain lengths 39-53 were 44% lower in abundance

261 than they were in the livers of normoxic rats (p = 0.002) and 48% lower than in the livers of 14 day

262 hypoxic rats (p = 0.0005) (**Figure 5D**). This contrasts with hepatic TAGs of longer chain lengths 54-62,

263 which were unchanged following hypoxic exposure (**Figure 5E**). Fragmentation analysis was

264 performed on the TAGs with the highest peak intensities to reveal their fatty acid compositions. This

265 included palmitic (16:0), palmitoleic (16:1), stearic (18:0) and oleic (18:1) acids (**Figure 5F-L**). TAGs with

266 these specific fatty acid compositions have been directly associated with hepatic *de novo* lipogenesis

267 (DNL) (44).

268 The fall in DNL-associated TAGs in response to 2 days of hypoxic exposure was driven by hypoxia rather

269 than the associated fall in food consumption, as in normoxic rats pair-fed to match those exposed to

270 hypoxia there was a 41% increase (p = 0.07) in TAGs of 39-53 chain length and a 70% increase (p =

271 0.007) in TAGs of 54-62 chain lengths (**Additional File 1: Figure S6A,B**).

272 To probe the effects of mild CIII inhibition on lipid homeostasis in short term hypoxia, the lipid profiles

273 of Veh and GSK932121A-treated animals following 2 days of hypoxia were compared. An OPLS-DA

274 model readily separated these groups (R^2X(cum) = 50.6%, Q^2(cum) = 69.3%), (**Additional File 1: Figure**

275 **S7A**), and the model passed cross-validation by random permutation (**Additional File 1: Figure S7B),**

276 y-axis intercepts R^2 = 0.0, 0.907 Q^2 = 0.0, -0.339) and by CV-ANOVA (p = 0.049). Key discriminants from

277 this model, identified using the same S plot method as outlined above, were TAGs with 37-47 and 60-

278 65 carbon chain lengths (**Additional File 1: Figure S7C**). This suggests that the enhanced respiratory

279 capacity in response to short-term hypoxia influences the hepatic lipid profile, in particular the

280 composition of the TAG pool. Mild CIII inhibition with GSK932121A did not, however, affect the fall in

281 DNL-associated TAGs after 2 days of hypoxia, as GSK932121A-treated animals displayed a 46%

282 decrease in TAGs of chain lengths 39-53 in comparison with normoxic animals (p = 0.01) (**Additional**

283 **File 1: Figure S7D**). Moreover, GSK932121A administration induced a fall in abundance of these TAGs

284 after 14 d hypoxia by 14% (p = 0.04). As with the Veh-treated animals, no change was observed in

285 TAGs of 54-62 chain lengths with GSK932121A treatment (**Additional File 1: Figure S7E**).

286 Lipid abundance was consistently higher in the livers of normoxic, GSK932121A-treated rats compared

287 with normoxic, Veh-treated rats. This was apparent in TAG levels (**Figure 5 D,E** and **Additional File 1:**

288 **Figure S7D,E**), cardiolipin (**Figure 2G**) and in total lipid abundance (**Additional File 1: Figure S7F**), the

289 latter being 36% higher in normoxic, GSK932121A-treateded animals compared to Veh (p < 0.01). No

290 comparable response to GSK932121A treatment was seen in either hypoxic group. This suggests that

291 hepatic lipid homeostasis is disrupted in response to mild CIII inhibition, with the rise in total liver lipid

292 intensity implying enhanced lipogenesis. However, this response was absent in the livers of hypoxic

293 rats, perhaps suggesting that it is dependent upon an ample O_2 supply.

294

Discussion

295 **Discussion**

296 Hypoxia is a key feature of common hepatic pathologies, with the time dependent nature of the

297 hepatic metabolic response to hypoxia being critical to our understanding of the aetiology of these

298 conditions. Here, we report that hepatic respiratory capacity is enhanced following acute hypoxic

299 exposure. This response was sensitive to mild CIII inhibition, which suppressed this rise in respiratory

300 capacity and disrupted metabolic homeostasis. Hepatic mitochondrial content was unaltered by

301 hypoxia, but instead, an increased abundance of mitochondrial supercomplexes, complex IV monomer

302 and associated factors may underlie this enhanced respiratory capacity. Short-term hypoxia resulted

303 in the accumulation of hepatic and plasma acyl-carnitines and other alterations to the hepatic lipid

304 profile, including depletion of TAGs associated with DNL. The rise in respiratory capacity, increased

305 sensitivity to CIII inhibition, and alterations to TAG profile were all transient, with each returning to

306 normoxic levels following systemic acclimation after 14 days of hypoxia.

307 A strength of our study is the use of a tightly-controlled rat model of hypoxic exposure, which shows

308 physiological acclimation over a time course that has been defined previously (22). Whilst the acute

309 suppression of food intake upon hypoxic exposure can be a confounder in metabolic studies of this

310 model (22), the inclusion of pair-fed normoxic animals in this study allowed us to separate the effects

311 of a reduction in food intake from hypoxia *per se*. An additional strength of this study was the novel

312 use of a CIII inhibitor with a well-understood toxicity profile (21, 23) in order to mechanistically

313 investigate the role of the respiratory chain in the response to hypoxia.

314 We adopted multiple techniques to comprehensively assess the metabolic response to hypoxia,

315 including targeted metabolomics and lipid profiling alongside detailed mitochondrial phenotyping.

316 Our method for evaluating mitochondrial respiration utilises tissue homogenates, which can limit

317 sensitivity in comparison with the use of isolated mitochondria. However, this approach allowed for

318 swift preparation and minimised washout of the CIII inhibitor.

13

319 Within the 2 day period of hypoxic exposure, systemic adjustments to mitigate the fall in O_2 delivery

320 are yet to fully occur, and we saw no change in [Hb] within this timeframe. This period of acute hypoxic

321 stress therefore represents a metabolic challenge for tissues such as liver. At this timepoint enhanced

322 OXPHOS capacity, potentially supported by an increase in mitochondrial supercomplex formation,

323 occurs alongside downregulation of the oxygen-consuming process of DNL. This enhanced OXPHOS

324 capacity appears to support metabolic homeostasis, with no change in expression of glycolytic

325 enzymes or intermediates or of glycogen stores suggesting that at this timepoint there is no greater

326 reliance on glycolytic flux for energetic homeostasis. Instead, suppression of the enhanced respiratory

327 capacity via mild inhibition of CIII resulted in increased levels of glycolytic intermediates, underlining

328 the importance of this enhanced capacity in maintaining oxidative metabolism. This therefore

329 suggests enhanced respiratory capacity is necessary to prevent dependence upon glycolysis and

330 maintain energetic homeostasis. This is in line with previous work in rodent heart and human skeletal

331 muscle where metabolic adjustment to hypoxic exposure served to maintain tissue energetics (14,

332 45).

333 The increased OXPHOS capacity, and accompanying non-significant trend towards enhanced fatty acid

334 oxidation capacity, does not fully compensate for the metabolic stress induced by acute hypoxia, with

335 accumulation of hepatic long-chain acyl-carnitines indicating impaired fatty acid oxidation. Acyl-

336 carnitines are derivatives of fatty acids required for transport across the inner mitochondrial

337 membrane. Tissue acyl-carnitine levels are therefore indicative of flux through fatty acid oxidation and

338 accumulation of long chain acyl-carnitines in hypoxia has previously been reported in the heart (46-

339 48), plasma (46) and skeletal muscle (45). Together with a decline in the expression of fatty acid

340 metabolising enzymes (45, 49) and fatty acid oxidation capacity (14, 45, 50) this supports the notion

341 of hypoxia-induced suppression of fat oxidation. Accumulation of acyl-carnitines may also result from

342 decreased TAG synthesis, which has been associated with onset of lipotoxicity (51, 52).

343 The non-significant trend towards increased fatty acid oxidation capacity we observe after 2 day

344 hypoxic exposure likely arose as a result of the acute suppression in food intake over this period.

14

345 Indeed, there was a greater (and statistically-significant) increase in fatty acid oxidation capacity in

346 rats pair-fed to match to the intake of hypoxic rats. This is in line with prior reports of elevated fatty

347 acid oxidation in response to calorie restriction (53), and may result from activation of peroxisome-

348 proliferator activated receptor α (PPARα) (54). Calorie restriction has also been attributed to

349 increasing ETS capacity upon the addition of FCCP (55, 56), an effect we too observed in the pair-fed

350 animals and which was maintained after 2 days of hypoxia. In our study, hypoxia appears to partly

351 suppress this acute increase in fatty acid oxidation that would otherwise be expected as a result of

352 the fall in food intake, and this corresponds with the hypoxic suppression of PPARα transcriptional

353 activity seen in other tissues (14, 22, 45). Fatty acid oxidation is supported through electron transfer

354 to complex I (via NADH) and the electron-transferring flavoprotein dehydrogenase (via free $FADH_2$),

355 however, complex II (succinate dehydrogenase) does also support fatty acid oxidation through its role

356 in the TCA Cycle. The increase in S-Pathway flux that we observed following 2 days of hypoxia, which

357 was not apparent in pair fed animals, could potentially impact on the capacity to oxidise fatty acids,

358 alongside other oxidative substrates. However, the increase in S-pathway flux also appears to be

359 insufficient to prevent long chain acyl-carnitine accumulation.

360 The findings of enhanced respiratory capacity, greater sensitivity to CIII inhibition, acyl-carnitine

361 accumulation and other lipid profile changes occurring after 2 days of hypoxic exposure were

362 transient, largely returning to normoxic levels following 14 days of hypoxic exposure. This suggests

363 that acclimatisation alleviates the hypoxic stress through improvements in systemic O_2 delivery. For

364 instance, haemoglobin concentration was increased following 14 days of hypoxia, a response

365 mediated by HIF-2α through induction of erythropoietin (57). Whilst the present work does not delve

366 further into the mechanisms of systemic acclimatisation that support hepatic metabolism with more

367 sustained hypoxia, this would be an interesting avenue for future investigation.

368 Our examination of respiratory supercomplexes identified an increase in density of bands

369 corresponding to supercomplexes $I+III_2$ and III_2+IV co-migrated with V_n following 2 days of hypoxic

370 exposure, alongside factors critical for supercomplex assembly, cardiolipin and *Cox7a2l* expression.

15

371 Each of these responses appeared to be unaffected by addition of the CIII inhibitor. This inhibitor has

372 been shown to impair catalytic activity of CIII (21, 23) and our results suggest it does not impact

373 supercomplex assembly. The aggregation of respiratory chain complexes into macromolecular

374 assemblies are thought to increase efficiency of electron flow between complexes and promote

375 complex stability (58). Supercomplex assembly has been shown to dynamically adapt to changes in

376 cellular metabolism (59). This has been demonstrated in human skeletal muscle, with formation of

377 complex I, III and IV containing supercomplexes decreasing in diabetic individuals (60), but increasing

378 in response to exercise training (32). In relation to hypoxia, sustained abundance of supercomplexes

379 was found to be necessary to maintain robust growth of pancreatic ductal adenocarcinoma under

380 conditions of extreme hypoxia (0.1% O_2), a response dependent upon functional CIII and CIV (61).

381 Hypoxia is also known to affect the expression of *Higd1a*, a transcriptional target of HIF1α (62, 63),

382 with increased levels being associated with cell survival in hypoxia (64). In line with this, we found an

383 increase in *Higd1a* expression following 2 days and 14 days of hypoxic exposure. However, given that

384 the rise in supercomplex abundance was only observed after 2 day hypoxia, the sustained increase

385 may link to other effects of *Higd1a* on respiratory chain performance. For instance, it has been shown

386 to bind the heme α active center to ensure optimal activity of CIV in hypoxia (65), and to incorporate

387 UQCRFS1 into CIII (66).

388 Our results demonstrate no change in supercomplex band density in response to reduced food intake

389 over the 2 day period. The response to reduced calorie intake may be time dependent, as the

390 proportion of CIII assembled with CI has been shown fall in response to 18 hours of starvation in mice

391 (58).

392 Our examination of the hepatic lipid profile revealed a depletion of TAGs selectively enriched for

393 palmitate, stearate and oleate, which have been associated with DNL (44, 67). This suggests

394 suppression of DNL in response to the short-term hypoxic insult. DNL is the synthesis of fatty acid

395 chains from acetyl CoA (AcCoA) derived from numerous metabolic reactions including glycolysis and

396 amino acid deamination. These fatty acids subsequently undergo condensation with glycerol to form

16

397 TAGs (68, 69). Elongation of the substrate acyl chain ceases at the 16 or 18 carbon stage, with palmitic

398 acid (C16) being the major product (70, 71). Palmitic acid can be utilised to form a range of fatty acids,

399 such as oleic acid through elongation to stearic acid followed by oxygen-dependent desaturation

400 catalysed by stearoyl-CoA desaturase (SCD)1 (72, 73). Examination of tumour-derived mammalian cell

401 lines (MDA-MB-468, HeLa and A549) following 72hrs in hypoxia (0.5-1% O_2) revealed a decrease in

402 SCD1 flux, a shift away from glucose-derived AcCoA towards glutamine-derived AcCoA, and an

403 increase in fatty acid import (73). Together, this implied DNL was bypassed in hypoxia (73).

404 An alternate hypothesis to explain the depletion of these specific hepatic TAG species at 2 days of

405 hypoxia includes dietary changes. In humans, high protein and carbohydrate intake has been

406 associated with inducing DNL (44, 74, 75), whilst calorie restriction has been reported to suppress

407 hepatic DNL (75). Here we observed an increase in TAGs of chain lengths 39-53 in pair-fed rats,

408 suggesting that the hypoxic driven changes in hepatic TAG composition are not due to decreased food

409 intake. The profile of these TAG species may also be affected by alterations in adipose tissue turnover.

410 Hypoxia has been associated with adipose tissue dysfunction, including impaired insulin-suppression

411 of lipolysis (76), decreased expression of genes associated with DNL (77) and suppression of

412 lipoprotein lipase activity alongside increased release of non-esterified fatty acids (78). In rats,

413 polyunsaturated fatty acids are the most abundant fatty acids and have the highest relative

414 mobilisation rate from adipose tissue (79, 80) , whereas monounsaturated and unsaturated fatty acids

415 are only moderately mobilised (79, 80). It is therefore unlikely that hypoxia induced changes in adipose

416 tissue turnover affect incorporation of fatty acids 18:1, 18:0, 16:1 and 16:0 into TAGs as we observe.

417 An interesting avenue for future research would be the effects of high fat feeding on the hepatic

418 hypoxic response. High fat feeding in rodents has been associated with the promotion of hypoxia

419 signalling and mitochondrial dysfunction in liver (81), whilst a high-fat diet exacerbated energetic

420 impairments in the hypoxic heart (14). The combination of a high-fat, high-cholesterol diet and chronic

421 intermittent hypoxia was associated with greater hepatic lipid peroxidation and inflammation (82).

17

422 The fatty acid composition of the diet used in any such manipulation would be of particular

423 importance, for instance given that supplementation of oleic acid has been shown to protect against

424 hepatic lipotoxicity induced by palmitic acid (83). Dietary manipulation such as this may help to probe

425 links between altered mitochondrial function and lipid metabolism at the hepatic and systemic level

426 in hypoxia. This could be of particular importance when considering nutritional strategies for

427 pathologies associated with systemic hypoxia, such as critical illness. Examination of skeletal muscle

428 and plasma from critically ill patients has demonstrated evidence of lipid accumulation in the first 48

429 hrs following admission to an intensive care unit, alongside impairment of fatty acid oxidation,

430 accumulation of muscle acyl-carnitines and diacylglycerol and plasma TAGs (84).

Conclusion

432 In conclusion, mitochondria play a critical role in the hepatic response to shorter-term hypoxic stress,

433 which is marked by a transient enhancement of respiratory capacity, associated with the formation of

434 mitochondrial supercomplexes. This enhanced respiratory capacity is essential for certain aspects of

435 metabolic homeostasis in the liver. Hepatic and systemic lipid metabolism is transiently disrupted by

436 shorter-term hypoxia, with hypoxia-induced alterations to hepatic TAG profiles being sensitive to

437 complex III inhibition. Thus, the liver responds to shorter-term hypoxia via changes in mitochondrial

438 respiratory function and lipid metabolism.

Methods

Experimental model

441 Female Crl:CD(SD) rats (Charles River Laboratories) 220-300 g were randomly assigned one of 6

442 experimental groups (n = 8-10 per group). Female rats were chosen as the hepatotoxicity profile of

443 GSK932121A is better understood in females than males (21). The study design is presented in **Figure**

444 **1A**. Rats were pair-housed in conventional cages in a temperature (23°C) and humidity-controlled

445 environment with a 12 h/12 h light/dark cycle. Rats were fed a standard diet (RM1(P), Special Diet

446 Services, UK) and had access to food and water *ad libitum*, with the exception of the group pair-fed to

18

447 match food intake of hypoxic animals as described below. Rats were randomly assigned either to

448 remain under normoxic conditions (21% O_2) or to be housed in hypoxia (10% O_2) in a flexible-film

449 chamber (PFI Systems Ltd., Milton Keynes, UK) for either 2 days or 14 days, with 20 air changes/h.

450 Body mass, food and water intake were measured daily. At the end of the hypoxic exposure period,

451 rats received an *i.p.* injection of either GSK932121A (a mitochondrial complex III inhibitor) or vehicle.

452 The chemical structure of GSK932121A has been described previously (21). The treatment comprised

453 a nanomilled and spray-dried formulation of GSK932121A (49.5% w/w) containing mannitol (44.5%

454 w/w), hydroxypropylmethylcellulose pharmacoat 603 (5% w/w) and sodium lauryl sulphate (1% w/w)

455 suspended in sterile water. The vehicle was identical in formulation minus GSK932121A. A dosing

456 concentration of 25 mg kg^{-1}, expressed in terms of the parent compound, was administered.

457 Following administration, clinical signs were monitored every 15-30 mins. The following were

458 measured on a scale of 0-2, with 0 being not present, 1 obvious presentation and 2 more severe

459 presentation: degree of piloerection, hyperventilation, orbital tightening and subdued behaviour (24).

460 The point of termination was determined by the severity of clinical signs and did not exceed 3 h post-

461 injection. Rats were anaesthetised by *i.p.* injection of pentobarbital (Euthatal, Merial), at a dose of

462 500 mg kg^{-1} body mass. After cessation of peripheral sensitivity, the chest cavity was opened, and

463 blood was collected from the left ventricle by cardiac puncture and transferred to an EDTA vacuette

464 tube (K3 EDTA, Greiner Bio-one). A droplet was taken from this collection and used to measure blood

465 glucose (Accu-Chek Compact Plus glucometer, Roche, Switzerland). Meanwhile, a droplet of blood

466 taken from the tail vein was loaded into a microcuvette for quantification of haemoglobin

467 concentration using a HemoCue Hb201 Analyzer (Ängelholm, Sweden).

468 The left lateral lobe of the liver was excised, and a portion placed into ice-cold biopsy preservation

469 medium (BIOPS: 2.77 mM CaK_2EGTA, 7.23 mM K_2EGTA, 6.56 mM $MgCl_2.6H_2O$, 20 mM taurine, 15 mM

470 phosphocreatine, 20 mM imidazole, 0.5 mM dithiothreitol, 50 mM MES, 5.77 mM Na_2ATP, pH 7.1) for

471 analysis by high-resolution respirometry. A further section was diced and placed into fixative for

19

472 electron microscopy (EM). The remainder was snap-frozen in isopentane cooled on dry ice and stored

473 at -80°C. All liver work described was performed on the left lateral lobe. To obtain plasma for

474 metabolomics, whole blood collected was spun at 2000 x g for 10 mins at 4°C and the plasma layer

475 removed.

476 Animals pair-fed to match the food intake of hypoxic rats were also female Crl:CD(SD) rats (220-300

477 g), and were single-housed in normoxia (n = 6/group) in conventional cages in a temperature (23°C)

478 and humidity-controlled environment with a 12 h/12 h light/dark cycle, as described above. They were

479 fed a standard diet (RM1(P), Special Diet Services, UK) and had access to water *ad libitum*. Rats were

480 randomly assigned to a control group fed *ad libitum* or pair-fed to match the intake observed over 2

481 day hypoxic exposure: 10 g for the first 24 hours, 14 g for the second 24 hours. Termination and

482 collection of the liver were performed as described above.

483 *Blood lactate*

484 Within 30 min of blood collection, whole blood was added to tricarboxylic acid (0.6 N) at a ratio of 1:3

485 and vortexed thoroughly. Blood lactate was assessed as described previously (21).

486 *Ultraperformance liquid chromatography (UPLC) for GSK932121A detection*

487 Snap-frozen liver (100-200mg) was homogenised using Precellys Tissue Homogeniser (Bertin

488 Instruments) in water to give a 1:3 (w/v) sample using 3 x 30 second cycles at 6500rpm. For extraction,

489 10µl of sample was added to internal standard working solution (ISWS, 10ng/mL [$^{13}C_6$]-GSK932121A

490 in Acetonitrile), vortexed and centrifuged for 15 minutes at 3000g. Snap frozen plasma (50µl) was

491 extracted using 25ng/mL ISWS. UPLC analysis was performed using AQUK35 (Waters Acquity) UPLC

492 system (Agilent, United States) coupled with UK22-AB/Sciex API4000 (Sciex, United States) using

493 Positive-ion TurboIonSpray® (Sciex). The assay was run over 1.5 minutes using a 50 x 2.1mm BEH C18

494 1.7 µm column (Waters^{TM} Acquity) conditioned at 50°C with a flow rate of 0.8mL/min and 0.5µl of

495 sample. The mobile phase consisted of: (A) HPLC grade water, 0.1% formic acid and (B) Acetonitrile.

496 GSK932121A analyte precursor and product ions were detected at 426.1 m/z and 231.1 m/z

497 respectively at 1 min retention time. Analysis was performed using Analyst 1.4.1 (Sciex).

498 *Liver glycogen*

499 Snap-frozen liver was prepared and analysed using a glycogen assay kit (Abcam, ab65620) following

500 manufacturer's instructions. Values were corrected to protein concentration obtained from a

501 bicinchoninic acid (BCA) assay (BCA1-1KT, Sigma).

502 *Liver high-resolution mitochondrial respirometry*

503 The BIOPS-preserved liver sample was prepared for respirometry as described previously (85).

504 Respiration rates were analysed using a substrate-uncoupler inhibitor titration in duplicate on each

505 biological replicate. J_{O2} was measured following the addition of octanoyl-carnitine (0.2 mM) and

506 malate (1 mM) initially in the LEAK state i.e. without ADP (OctM$_L$), and then in the OXPHOS state

507 following the addition of ADP (10 mM) (OctM$_P$). The N-pathway via complex I was then stimulated

508 with the addition of glutamate (10 mM) (GM$_P$), followed by cytochrome *c* (10 μM) to assess outer

509 mitochondrial membrane integrity. Maximal OXPHOS was then stimulated with addition of succinate

510 (10 mM) (GMS$_P$). Stimulation of maximal electron transfer system (ETS) capacity was achieved through

511 the addition of carbonyl cyanide-p-trifluoromethoxyphenylhydrazone (FCCP) (titrated in 0.5 μM

512 additions until maximal capacity was reached) (GMS$_E$). Finally, complex I was inhibited through the

513 addition of rotenone (0.5 μM), restricting electron flux to the S-pathway via complex II (S$_E$). Respiration

514 rates were normalised to wet mass of liver tissue.

515 *Citrate synthase activity*

516 Snap-frozen liver was prepared and analysed for citrate synthase activity as described previously (86).

517 *Metabolomics/lipidomics*

21

518 A chloroform/methanol extraction was performed on snap-frozen liver (~30 mg) and plasma (20 µl)

519 as described previously (45) followed by ultra-high performance liquid chromatography mass

520 spectrometry (87, 88).

521 The aqueous phase underwent normal and reverse phase analysis. The aqueous and organic fractions

522 were combined for carnitine analysis. The protein pellet was re-suspended in RIPA buffer

523 (ThermoScientific) containing protease inhibitor (Roche) and the protein concentration determined

524 using a BCA assay (BCA1-1KT, Sigma). Data were processed using the vendor's software and

525 normalized to protein concentration and to the intensity of internal standards.

526 *Aqueous metabolite analysis*

527 Reverse phase analysis was performed as described previously (88). Before the analysis, samples were

528 reconstituted in 0.1 mL of a 10 mM ammonium acetate water solution containing a mixture of 8

529 internal standards at the concentration of 10 µM (D3 - proline, D8-valine, D10-leucine, U-^{13}C lysine,

530 ^{13}C-glutamic acid, D5-phenylalanine and, D3-succinic acid and D4- serotonin). Normal phase analysis

531 was performed using a Thermo Scientific Vanquish^{TM} UHPLC^{+} series coupled with a TSQ Quantiva mass

532 spectrometer (Thermo Fisher Scientific, Waltham, Massachusetts, United States) and was used with

533 an electron spray ionisation (ESI) source, operated in positive and negative ion mode with polarity

534 switching. The electrospray voltage was set to 3500 V for the positive ionisation and to 2500 V for the

535 negative ionisation. N_2 at 48 mTorr and 420°C was used as a drying gas for solvent evaporation. The

536 aqueous phase was analysed with a BEHAmide (150 x 2.1 mm 1.7 µm) column. The column was

537 conditioned at 30°C. The mobile phase consisted of: (A) a 0.1 M of aqueous solution of ammonium

538 carbonate and (B) acetonitrile. The mobile phase was pumped at a flow rate of 600 µL/min

539 programmed as follows: initially at 20% of A for 1.5 min, then subjected to a linear increase from 20%

540 to 60% of A over 2.5 min and kept at this percentage for 1 min before being brought back to initial

541 conditions after 0.1 min, followed by 3 min of equilibration. Xcalibur software (Thermo Fisher Scientific

542 version 4.1, Waltham, Massachusetts, United States) was used for data acquisition. Putative

543 recognition of all detected metabolites was performed using a targeted MS/MS analysis. Before the

544 analysis, samples were reconstituted in 0.1 mL of acetonitrile: 1 M aqueous ammonium carbonate

545 solution (7:3 v/v) containing a mixture of 3 internal standards at the concentration of 10 μM (^{13}C-

546 glutamic acid, D3-succinic acid and AMP).

547 *Carnitine analysis*

548 Samples were prepared as described previously (45, 85). A Thermo scientific UHPLC$^+$ series coupled

549 with a TSQ Quantiva mass spectrometer (Thermos fisher scientific, Waltham, Massachusetts, United

550 States) and was used with an ESI source, operated in positive and negative ion mode at the same time.

551 The electrospray voltage was set to 3500 V for the positive ionisation and to 2500 V for the negative

552 ionisation. N_2 at 48 mTorr and 420°C was used as a drying gas for solvent evaporation. The combined

553 aqueous and organic phases were analysed with an ACE Excel 2 C18 PFP (100A. 150 x 2.1 mm 5 μm)

554 column. The column was conditioned at 30°C. The mobile phase consisted of: (A) 0.1% of formic acid

555 water solution and (B) methanol solution. The mobile phase was pumped at a flow rate of 0.450

556 μL/min programmed as follows: initially stayed at 0.5% of B for 1 min, then subjected to a linear

557 increase from to 100% of A over 9 min and kept at this percentage for 2 min before being brought

558 back to initial conditions after 0.1 min. Xcalibur software was used for data acquisition. Putative

559 recognition of all detected metabolites was performed using a targeted MS/MS analysis. Before the

560 analysis, the combined carnitine fraction was reconstituted in 0.1 mL of a methanol: water solution

561 (4:1 v/v) containing an internal standard mix of eight deuterated carnitines at a concentration of 2 μM

562 (free carnitine, C2, C3, C4, C5, C8, C14, C16).

563 *Lipidomics*

564 A chloroform/methanol extraction was performed, as stated above for liver, as well as on 20 μl snap

565 frozen plasma. For both liver and plasma, the dried organic fraction was reconstituted in 50 μL of

23

566   methanol/chloroform (1:1) and vortexed thoroughly. 10 μL of the sample was then diluted into 190

567   μL of isopropyl alcohol/acetonitrile/water (2:1:1) and briefly vortexed.

568   An LTQ Orbitrap Elite Mass Spectrometer (Thermo Fisher Scientific) was used in positive and negative

569   modes. Metabolites were ionised by heated electrospray before entering the spectrometer. The

570   source temperature was set to 420°C, and the capillary temperature to 380°C. In positive mode, the

571   spray voltage was set to 3.5 kV, while in negative it was 2.5 kV. Data was collected using the Fourier

572   transform mass spectrometer (FTMS) analyser. The resolution was set to 60,000 and the data was

573   obtained in profile mode. The full scan was performed across an m/z range of 110-2000. For both

574   modes, 5 μL of sample was injected onto a C18 CSH column, 2.1 x 50 mm (1.7 μM pore size) (Waters),

575   which was held at 55°C using an Ultimate 3000 UHPLC system (Thermo Fisher Scientific). The mobile

576   phase comprise solvents A (acetonitrile/water 60:40) and B (acetonitrile/isopropanol 10:90), run

577   through the column in a gradient (40% B, increased to 43% B after 0.8 min, 50% B at 0.9 min, 54% B

578   at 4.8 min, 70% B at 4.9 min, 81% B at 5.8 min, raised to 99% B at 8 min for 0.5 min before returning

579   to 40% for 1.5 min). Total run time was 10 min, with a flow rate of 0.500 μL/min. In positive mode, 10

580   mM ammonium formate was added to solvents A and B. In negative mode, 10 mM ammonium acetate

581   was the solvent additive. Solvent additives were chosen based on previous work (89). Before analysis,

582   250 μl internal standard (IS) mix was added to each sample. This was composed of deuterated

583   standards sourced from Avanti Polar Lipids (C16-d31 Ceramide, 16:0-d31-18:1 PA,16:0-d31-18:1 PC,

584   16:0-d31-18:1 PE, 16:0-d31-18:1 PG, 16:0-d31-18:1 PI,14:0 PS-d54, and 16:0-d31 SM) and CDN

585   Isotopes/QMX Laboratories (18:0-d6 CE, 15:0-d29 FA, 17:0-d33 FA, 20:0-d39 FA, 14:0-d29 LPC-d13,

586   45:0-d87 TG, 48:0-d83 TG, and 54:0-d105 TG). IS mix was made in 1:1 methanol chloroform, and each

587   standard was at 2.5 μg/mL.

588   For processing, spectra were converted to .mzML files using MSConvert (Proteowizard) for subsequent

589   analysis. XCMS software within R was used to process data and identify peaks. Peaks were identified

590   based on an approximate FWHM of 5 sec and a signal-to-noise threshold of 5. To improve peak

591   identification, peaks had to be present in a minimum of 25% of the samples. Peaks were annotated by

592 accurate mass and retention time using an in-house R script and comparison to the LipidMaps

593 database (90). Peak intensity was normalised to internal standards and, in the instance of liver, to

594 protein concentration.

595 *Fragmentation analysis*

596 Triacylglycerol chain composition was analysed using a data-dependent acquisition (DDA)-based

597 fragmentation step. Ions were fragmented using collision induced dissociation (CID) at a normalised

598 collision energy of 35. Precursor ions were selected from a mass list, with the most intense ion on the

599 list fragmented in each scan. The minimum signal required was 5000 counts and the isolation width

600 set to 1. The activation time was 10 ms and the activation Q set to 0.25. Fragmentation spectra were

601 acquired in centroid mode at a resolution of 15,000 using the FTMS analyser. Lipid identity was

602 determined through manual identification of fragmentation patterns according to published methods

603 (91), a process aided by use of an online resources http://www.byrdwell.com/Triacylglycerols/.

604 For both positive and negative ionisation modes, 5 μL of sample was injected onto a C18 CSH column,

605 75 μM x 100 mm (Waters, 186005297), which was held at 55°C using an Ultimate 3000 UHPLC system

606 (Thermo Fisher Scientific). The mobile phase comprise solvents A (acetonitrile/water 60:40) and B

607 (acetonitrile/isopropanol 10:90), run through the column in a gradient (40% B, increased to 43% B

608 after 2 min, 50% B at 2.1 min, 54% B at 12 min, 70% B at 12.1 min, raised to 99% B at 18 min before

609 returning to 40% for 2 min). Total run time was 20 min, with a flow rate of 0.400 μL/min. In positive

610 mode, 10 mM ammonium formate (Fisher Scientific, A/3440/53) was added to solvents A and B. In

611 negative mode, 10 mM ammonium acetate (Sigma Aldrich, 516961) was the solvent additive.

612 <u>*Transmission electron microscopy*</u>

613 Samples of liver were fixed in 4% Formaldehyde/1% Glutaraldehyde, washed in Millonig's Phosphate

614 buffer and transferred to a Leica EMTP automatic tissue processor (Leica Microsystems). Tissues were

615 post-fixed in 2% Osmium Tetroxide and processed into Agar 100 Epoxy resin (Agar Scientific). Samples

616 were embedded and allowed to polymerise overnight at 60°C. From the resulting blocks semi-thin (1

617 μM thick) sections were cut on a Leica UC6 Ultra-microtome (Leica Microsystems) and stained with

618 Toluidine Blue to locate the correct region using light microscopy. Subsequently Ultra-thin (80-90 nm

619 thick) sections were cut and contrasted using 2% Lead Citrate and Uranyless stain (TABB). Grids were

620 examined using a Hitachi H7500 Transmission Electron Microscope (Hitachi High-tech) operating at 80

621 kV and images taken on a Gatan OneView Digital Camera (Gatan, Inc). Mitochondrial number was

622 quantified in images taken at x7000 magnification through a manual count, corrected to image area.

623 *Blue native polyacrylamide gel electrophoresis (BN-PAGE)*

624 Snap-frozen liver samples (~20 mg) were prepared and BN-PAGE performed as previously described

625 (31) with the addition of NativeMark™ unstained protein standard (Invitrogen, LC0725). Following BN-

626 PAGE, the gel was stained using a Colloidal Blue Staining kit (Invitrogen, LC6025) as per manufacturer's

627 instructions. The gel was then washed overnight in ddH$_2$O prior to imaging using HP Scanjet G4050

628 and analysis using ImageJ software (92). Band density was corrected to CII, as described previously

629 (60). Band identification was based on immunoblotting and comparison to prior work utilising this

630 approach in rodent liver (31). Immunoblotting was performed after transfer of unstained gels, as

631 previously described (31). After 50 minutes incubation in blocking buffer (5% Bovine Serum Albumin

632 (Sigma, A6003) TBS-T), staining of the individual complexes was achieved through overnight

633 incubation at 4°C with one of the following primary antibodies diluted in blocking buffer: NDUFA9

634 (Invitrogen, Cat#459100, RRID:AB_2532223, 2:1000), SDHA (Invitrogen, Cat#459200,

635 RRID:AB_2532231, 1:10,000), UQCRC2 (Abcam, ab14745, RRID: AB- 2213640 1:1000) MTCO1 (Abcam,

636 ab14705, RRID:AB_2084810, 1:1000), ATP5A (Abcam, ab14748 RRID:AB_301447, 1:1000). The

637 membrane was incubated with secondary antibody (Rabbit anti-Mouse IgG HRP, #61-6520, Invitrogen;

638 RRID:AB_2533933 1:10,000 in TBS-T)) for 1hr at room temperature, before ECL detection (Milipore)

639 and imaging using iBright 1500 (ThermoFisher Scientific).

640 Anti-OXPHOS antibody cocktail (Thermo Fisher Scientific, Cat#45-8099, RRID:AB_2533835) was also

641 used, followed by secondary antibody as above and staining using Immobilon™ Western

642 Chemiluminescent HRP Substrate (Millipore). To gain clearer resolution of the CII band, the membrane

643 was washed overnight using Tris buffered saline (TBS) –Tween and incubated with SDHA monoclonal

644 antibody (Invitrogen, Cat#459200, RRID:AB_2532231, 1:10,000).

645 Original immunoblot images for BN-PAGE gels are presented in **Additional File 1: Figure S8.** Original

646 colloidal blue staining images are presented in **Additional File 1: Figure S9.**

647 *Immunoblotting for OXPHOS complexes*

648 Preparation of tissue lysate was carried out as described previously (93). From this, 10ug protein was

649 loaded into 4-20% gradient gels (Mini-PROTEAN® TGX™ Precast Protein Gels, 15-well, 15 µl #4561096,

650 BioRAD) alongside a protein ladder (Precision plus protein dual color standards #1610374, BioRAD).

651 The gel was transferred to nitrocellulose membrane and this was stained in Ponceau S. The membrane

652 was blocked in 5% Skimmed milk-TBS-T for 1 hr prior to primary antibody incubation (Total OXPHOS

653 antibody cocktail, ab110412, Abcam, RRID:AB_2847807; 1:500 in 1% Milk TBS-T) overnight at 4°C. The

654 membrane was incubated with secondary antibody (Rabbit anti-Mouse IgG HRP, #61-6520, Invitrogen;

655 RRID:AB_2533933 1:5000 in TBS-T)) for 1hr at room temperature, before ECL detection (Milipore) and

656 imaging using iBright 1500 (ThermoFisher Scientific). Band density was quantified using Image J

657 software (92). The original immunoblot image is presented in **Additional File 1: Figure S8H.**

658 *Gene expression analysis*

659 Total RNA was extracted from frozen liver (~20 mg) using a RNeasy Plus Universal Mini Kit (QIAGEN),

660 as per manufacturer's instructions. The concentration of eluted RNA was measured using a Nanodrop

661 DN-1000 spectrophotometer. cDNA synthesis was carried out using the qScript synthesis kit, following

662 the manufacturer's protocol (Quantabio). mRNA expression was measured by quantitative (Q)-PCR

663 using SYBR Green Mastermix (Eurogentec Ltd.) and the DNA Engine Opticon 2 system (BioRad).

664 Primers were obtained from QuantiTech Primer Assay (QIAGEN) and product details are as follows:

665 Rn_Hk2_1   QT00190764,   Rn_Pfkl_1   QT00175651,   Rn_Ldha_2   QT02336243,   Rn_Higd1a_1

27

666 QT00372428, Rn_Stoml2_1 QT01571724 , Rn_Slc25a11_1 QT01082914 , Rn_Actb_1 QT00193473. In

667 the instance of Cox7a2l, QuantiFast SYBR Green PCR kit (QIAGEN) and QuantStudio 1 Real-Time PCR

668 System (Applied Biosystems, Thermo Fisher) were used. The primer was obtained from QuantiTect

669 Primer Assays (QIAGEN) with the following product details: Rn_Cox7a2l_1_SG. In all cases, transcript

670 levels were normalised to levels of *Actb* and fold change determined using the $2^{-\Delta\Delta CT}$ method, with

671 expression in vehicle/normoxic animals normalised to 1.

Quantification and statistical analysis

673 For comparisons between the effects of hypoxia and GSK93121A treatment, a two-way ANOVA was

674 employed. In the instance of comparison between hypoxic treatment alone, a one-way ANOVA was

675 employed. Where significant differences were found, post-hoc pairwise comparisons were carried out

676 with a Tukey's correction. Correlation analysis was performed using simple linear regression. Analysis

677 was carried out using GraphPad Prism 8 software (GraphPad Software Inc.) and differences were

678 considered significant when $p \leq 0.05$. Where bar charts are used, data are presented as ± SEM.

679 In the instance of targeted metabolomics (aqueous fraction and carnitines), values were corrected to

680 internal standard and tissue protein concentration prior to ANOVA testing. A false discovery rate

681 correction was also employed (two-stage linear step-up procedure of Benjamini, Krieger and Yekutieli,

682 $Q = 5\%$, threshold p value ≤ 0.032) to account for application of multiple ANOVAs. A post-hoc Tukey's

683 test was performed following this to define significant interactions. For presentation in heatmaps,

684 data was normalised using autoscaling and generalised logarithm transformation using Metaboanalyst

685 (94).

686 For open-profile lipidomic analysis, multivariate analysis was adopted. Data was first normalised by

687 Pareto scaling and generalised logarithm transformation using Metaboanalyst. The strategy for this

688 analysis was informed by the metabolomics and respirometry, which indicated a marked metabolic

689 effect occurring following 2 days of hypoxic exposure. Lipid profiles were compared using orthogonal

690 partial least squares – discriminant analysis (OPLS-DA), carried out using SIMCA (version 15, Umetrics,

28

691 Umea, Sweden). The discriminants driving the separation in profiles were defined as those lying 2 SD

692 away from the mean on an S plot. For presentation in heatmaps, normalised data was used.

693 Percentage changes and related statistical testing were calculated from original peak intensity data

694 using either one-way ANOVA when comparing hypoxic effect only, or two-way ANOVA when

695 comparing hypoxic and GSK932121A-treatment effects. GraphPad Prism was used for this analysis

696 and data presentation.

697 For analysis of the effects of pair-feeding to match that consumed by the hypoxic animals, an unpaired

698 Student t test was employed to compare the control to the pair-fed.

699 **List of abbreviations**

700 BN-PAGE = blue native polyacrylamide gel electrophoresis

701 CPT1 = carnitine palmitoyl transferase 1

702 CI - V = respiratory chain complexes I-V

703 DNL = *de novo* lipogenesis

704 ETS = electron transfer system

705 Hb = haemoglobin

706 HIF = hypoxia inducible factor

707 LC-MS = liquid chromatography –mass spectrometry

708 OPLS-DA = orthogonal partial least squares – discriminant analysis

709 OXPHOS = oxidative phosphorylation

710 PPARα = peroxisome proliferator-activated receptor α

711 TAG= triacylglyerol

712 TCA = tricarboxylic acid

713   UPLC = ultra performance liquid chromatography

714   Veh = vehicle treatment

715   **Declarations**

716   *Ethics approval and consent to participate*

717   All animal work was ethically reviewed by GlaxoSmithKline and the University of Cambridge Animal

718   Welfare and Ethical Review Committee, and carried out under a project licence in accordance with the

719   Animals (Scientific Procedures) Act 1986. Procedures involving live animals were carried out by a

720   personal licence holder in accordance with these regulations.

721   *Consent for publication*

722   Not applicable

723   *Availability of data and materials*

724   The datasets supporting the results presented in this article are freely available via the Cambridge

725   University Repository: https://doi.org/10.17863/CAM.75680 (95). Raw metabolomics data have been

726   deposited to the EMBL-EBI MetaboLights database (96) with the identifier MTBLS3713. The complete

727   dataset can be accessed here: https://www.ebi.ac.uk/metabolights/MTBLS3713 (97).

728   *Competing Interests*

729   The authors declare that they have no competing interests.

749 **<u>Figure titles and legends</u>**

750 **Figure 1: Shorter-term hypoxic exposure enhances hepatic mitochondrial respiratory capacity**

751   A. Experimental design. Female Crl:CD(SD) rats (220-300g) were exposed to normoxia or hypoxia

752   (10% O_2) for either 2 days (2 d) or 14 days (14 d), after which an electron transfer system

753   complex III (CIII) inhibitor (GSK932121A, 25 mg kg^{-1}, *i.p.*) or vehicle (Veh) was administered.

754   B. Haemoglobin concentration ([Hb]) (g/L) obtained from the tail vein upon termination. Data

755   set includes both vehicle and GSK932121A-treated groups, n = 18 normoxic, n = 16 for all other

756   groups.

757   C-H. Respiration of liver homogenates from Veh and GSK932121A-treated rats in the following

758   states: Octanoyl carnitine and malate-supported (β-oxidation) respiration, without ADP ($OctM_L$)

759   (C) and with ADP ($OctM_P$) (D) to assess fatty acid oxidation. Stimulation of complex I-supported

760   respiration with the addition of glutamate (GM_P) (E). Stimulation of maximal OXPHOS following

31

761 the addition of succinate (GMS$_P$) (F) and maximal ETS capacity with the addition of the uncoupler

762 FCCP (GMS$_E$) (G). Finally, inhibition of complex I-supported respiration through the addition of

763 rotenone, restricting electron flux through complex II in the presence of the electron transfer

764 system uncoupler FCCP (S$_E$) (H). Respiration rates are corrected to wet mass of liver tissue added

765 to the chamber. n = 9 Veh normoxic rats, n= 8 Veh 2 d hypoxic, Veh and GSK932121A-treated 14

766 d hypoxic, n = 7 normoxic and 2 d hypoxic GSK932121A-treated rats.

767 I. Transmission electron microscopy of hepatic tissue at x2500 and x7000 magnifications.

768 J. Number of hepatic mitochondria per tissue area (μm^2) using transmission electron

769 microscopy. Data in Veh and GSK932121A-treated rats is combined, n = 5 normoxic, n= 8

770 hypoxic 2 d, n = 4 hypoxic 14 d.

771 K. Hepatic citrate synthase activity normalised to protein concentration. Data in Veh and

772 GSK932121A-treated rats is combined, n = 17 normoxic, n = 16 hypoxic 2 d and 14 d.

773 Data are presented as mean ± SEM, *p <0.05, ** p ≤ 0.01, *** p ≤ 0.001.

774 **Figure 2: Short-term hypoxia is associated with hepatic mitochondrial supercomplex formation**

775 A. Immunoblotting of blue native polyacrylamide gel electrophoresis (BN-PAGE) gel using

776 antibodies for each singular respiratory complex and the OXPHOS antibody cocktail to confirm

777 identity of bands presented in the gel stained with colloidal blue. To avoid over-saturation of

778 the bottom band, the Complex IV immunoblot is presented as two separate exposures.

779 B. Colloidal blue staining of a representative BN-PAGE gel, from which band density was

780 quantified.

781 C-F. Band intensity for the following mitochondrial complex and supercomplex stoichiometric

782 combinations: I+III$_2$ (C), III$_2$+IV comigrated with V$_n$ (D), alongside mitochondrial complexes I (E) and

783 IV (F). Where the number of associated complexes is unknown, n is used. All bands are corrected

784 to complex II levels. n = 10 Veh normoxic, n = 7 GSK932121A-treated 2 d and 14 d hypoxic, n = 8

785 for remaining groups.

786   G. Peak intensity of cardiolipin, measured by liquid chromatography-mass spectrometry,

787   corrected to internal standard and protein concentration. n = 9 Veh normoxic, n = 7

788   GSK932121A-treated normoxic, n = 6 GSK932121A-treated 14 d hypoxia, n = 8 for remaining

789   groups.

790   H. Expression levels of *Cox7a2l* measured by qPCR, presented as fold induction corrected to *Actb.*

791   n = 7 GSK932121A-treated 14 d hypoxia, n = 8 for all remaining groups.

792   Data are presented as mean ± SEM, *$p <0.05$, ** $p \leq 0.01$, *** $p \leq 0.001$.

Figure 3: Maintenance of hepatic energetic homeostasis during short-term hypoxic stress is dependent on enhanced hepatic respiratory capacity

795   Targeted metabolomics performed using LC-MS, including presentation of dihydroxyacetone

796   phosphate (DHAP), 2/3-phosphoglycerate (PG), acetyl CoA (AcCoA) and phosphocreatine

797   (PCr). Data obtained from the peak area ratio, corrected to internal standards and protein

798   concentration. For heatmap presentation, data was normalised using autoscaling and

799   generalised logarithm transformation. n = 9 Veh normoxic, n = 8 all remaining groups. The 2 d

800   hypoxic exposure with GSK932121A administration was defined as statistically significant

801   across all metabolites presented through use of a two-way ANOVA plus false discovery rate

802   correction (two-stage linear step-up procedure of Benjamini, Krieger and Yekutieli, Q = 5%,

803   threshold p value < 0.032), followed by a post-hoc Tukey's test ($p < 0.05$).

Figure 4: Plasma and liver acyl-carnitine profiles are altered by short-term hypoxia

805   A. Plasma acyl-carnitines and free carnitine, n = 10 Veh normoxic, n = 8 all remaining groups.

806   B. Liver acyl-carnitines and free carnitine, n = 9 Veh normoxic, n = 8 all remaining groups.

807   Intermediates in both panels were assessed by targeted metabolomics using liquid

808   chromatography-mass spectrometry. Data presented is peak intensity obtained from the peak

809   area ratio, corrected to internal standards and protein concentration and normalised using

810   autoscaling and generalised logarithm transformation. The 2 d hypoxic exposure was defined

811
1
2 812
3
4
5 813
6
7 814
8
9
10 815
11
12
13 816
14
15
16 817
17
18 818
19
20 819
21
22
23 820
24
25 821
26
27 822
28
29
30 823
31
32 824
33
34
35 825
36
37 826
38
39 827
40
41
42
43 828
44
45 829
46
47 830
48
49
50 831
51
52
53 832
54
55 833
56
57 834
58
59
60
61
62
63
64
65

811   as statistically significant across all metabolites presented through use of a two-way ANOVA

812   plus false discovery rate correction (two-stage linear step-up procedure of Benjamini, Krieger

813   and Yekutieli, Q = 5%, threshold p value < 0.032), followed by a post-hoc Tukey's test (p <

814   0.05).

815 **Figure 5: Hepatic triacylglycerol (TAG) composition is altered by short-term hypoxia with**

816 **suppression of TAGs associated with *de novo* lipogenesis**

817   A. Orthogonal partial least squares – discriminant analysis (OPLS-DA) of hepatic lipidomic profiles

818   of Veh-treated normoxic (green) and 2 d hypoxic (red) treated rats, with each dot representing

819   the lipidomic profile of one animal. Data was obtained from the peak area ratio of LC-MS

820   analysis, corrected to internal standards and protein concentration and normalised using

821   Pareto Scaling and generalised logarithm transformation.

822   B. Permutation validation of the plot in panel A.

823   C. S-plot corresponding to the OPLS-DA model in panel A. Triacylglycerol species with

824   discriminatory values, defined as those lying 2 standard deviations from the mean, are

825   highlighted in orange.

826   D. Total peak intensities of TAGs with chain lengths 39-53.

827   E. Total peak intensities of TAGs with chain lengths 54-62.

828 F-L. Peak intensities of TAGs with the greatest peak intensities, alongside corresponding fatty acid

829 composition derived from fragmentation analysis where 16:0 denotes palmitic acid, 16:1

830 palmitoleic acid, 18:1 oleic acid, 18:0 stearic acid.

831 Data presented in panels C-L are Veh-treated animals in normoxia, after 2 d hypoxia and 14 d

832 hypoxia. Peak intensities are corrected to internal standard and protein concentration. Bar graphs

833 are presented as mean ± SEM, * p < 0.05, ** p ≤ 0.01, *** p ≤ 0.001. n = 9 Veh normoxic, n = 8 all

834 remaining groups.

835   **Additional File 1: Supplementary Figure legend titles**

836   **Additional File 1: Fig S1. Systemic and hepatic effects of GSK932121A administration.**

837   **Additional File 1: Fig S2. Food intake and body weights for Veh and GSK932121A treated animals,**
838   **alongside hepatic mitochondrial respiration rates from control and hypoxic pair-fed animals.**

839   **Additional File 1: Fig S3. BN-PAGE band identification and band intensity quantification for control**
840   **and hypoxic pair-fed animals.**

841   **Additional File 1: Fig S4. Protein expression of mitochondrial respiratory chain complexes and gene**
842   **expression of factors associated with mitochondrial supercomplex formation.**

843   **Additional File 1: Fig S5. Glycolytic gene expression.**

844   **Additional File 1: Fig S6. Effect of hypoxia pair-feeding on hepatic TAGs.**

845   **Additional File 1: Fig S7. Lipidomic profile of 2 d hypoxic Veh and GSK932121A treated animals,**
846   **TAG levels with GSK932121A treatment and total lipid intensity.**

847   **Additional File 1: Fig S8. Original immunoblot images.**

848   **Additional File 1: Fig S9. Original colloidal blue stained images obtained using BN-PAGE**

849

850

851

852 **References**

853 1.   Murray AJ, Montgomery HE, Feelisch M, Grocott MPW, Martin DS. Metabolic adjustment to
854 high-altitude hypoxia: from genetic signals to physiological implications. Biochemical Society
855 Transactions. 2018;46(3):599-607.10.1042/bst20170502
856 2.   Suzuki T, Shinjo S, Arai T, Kanai M, Goda N. Hypoxia and fatty liver. World J Gastroenterol.
857 2014;20(41):15087-97.10.3748/wjg.v20.i41.15087
858 3.   Mesarwi OA, Loomba R, Malhotra A. Obstructive Sleep Apnea, Hypoxia, and Nonalcoholic
859 Fatty Liver Disease. American Journal of Respiratory and Critical Care Medicine. 2019;199(7):830-
860 41.10.1164/rccm.201806-1109TR
861 4.   Semenza GL. Hypoxia-Inducible Factors in Physiology and Medicine. Cell. 2012;148(3):399-
862 408.https://doi.org/10.1016/j.cell.2012.01.021
863 5.   Lee P, Chandel NS, Simon MC. Cellular adaptation to hypoxia through hypoxia inducible
864 factors and beyond. Nature reviews Molecular cell biology. 2020;21(5):268-83.10.1038/s41580-020-
865 0227-y
866 6.   Guzy RD, Hoyos B, Robin E, Chen H, Liu L, Mansfield KD, et al. Mitochondrial complex III is
867 required for hypoxia-induced ROS production and cellular oxygen sensing. Cell Metabolism.
868 2005;1(6):401-8.https://doi.org/10.1016/j.cmet.2005.05.001
869 7.   Guzy RD, Schumacker PT. Oxygen sensing by mitochondria at complex III: the paradox of
870 increased reactive oxygen species during hypoxia. Exp Physiol. 2006;91(5):807-
871 19.10.1113/expphysiol.2006.033506
872 8.   Hamanaka RB, Weinberg SE, Reczek CR, Chandel NS. The Mitochondrial Respiratory Chain Is
873 Required for Organismal Adaptation to Hypoxia. Cell Reports. 2016;15(3):451-
874 9.https://doi.org/10.1016/j.celrep.2016.03.044
875 9.   Hernansanz-Agustín P, Ramos E, Navarro E, Parada E, Sánchez-López N, Peláez-Aguado L, et
876 al. Mitochondrial complex I deactivation is related to superoxide production in acute hypoxia. Redox
877 Biol. 2017;12:1040-51.10.1016/j.redox.2017.04.025
878 10.   Hernansanz-Agustín P, Choya-Foces C, Carregal-Romero S, Ramos E, Oliva T, Villa-Piña T, et
879 al. Na+ controls hypoxic signalling by the mitochondrial respiratory chain. Nature.
880 2020;586(7828):287-91.10.1038/s41586-020-2551-y
881 11.   Thomas LW, Ashcroft M. Exploring the molecular interface between hypoxia-inducible factor
882 signalling and mitochondria. Cellular and molecular life sciences : CMLS. 2019;76(9):1759-
883 77.10.1007/s00018-019-03039-y
884 12.   Papandreou I, Cairns RA, Fontana L, Lim AL, Denko NC. HIF-1 mediates adaptation to hypoxia
885 by actively downregulating mitochondrial oxygen consumption. Cell Metabolism. 2006;3(3):187-
886 97.https://doi.org/10.1016/j.cmet.2006.01.012
887 13.   Kim JW, Tchernyshyov I, Semenza GL, Dang CV. HIF-1-mediated expression of pyruvate
888 dehydrogenase kinase: a metabolic switch required for cellular adaptation to hypoxia. Cell Metab.
889 2006;3(3):177-85.10.1016/j.cmet.2006.02.002
890 14.   Cole MA, Jamil AHA, Heather LC, Murray AJ, Sutton ER, Slingo M, et al. On the pivotal role of
891 PPARα in adaptation of the heart to hypoxia and why fat in the diet increases hypoxic injury. The
892 FASEB Journal. 2016:fj. 201500094R
893 15.   Formenti F, Constantin-Teodosiu D, Emmanuel Y, Cheeseman J, Dorrington KL, Edwards LM,
894 et al. Regulation of human metabolism by hypoxia-inducible factor. Proceedings of the National
895 Academy of Sciences 2010;107(28):12722-7.10.1073/pnas.1002339107
896 16.   Perrotta S, Roberti D, Bencivenga D, Corsetto P, O'Brien KA, Caiazza M, et al. Effects of
897 Germline VHL Deficiency on Growth, Metabolism, and Mitochondria. New England Journal of
898 Medicine. 2020;382(9):835-44.10.1056/NEJMoa1907362
899 17.   Rankin EB, Rha J, Selak MA, Unger TL, Keith B, Liu Q, et al. Hypoxia-inducible factor 2
900 regulates hepatic lipid metabolism. Mol Cell Biol. 2009;29(16):4527-38.10.1128/MCB.00200-09

18.   Nishiyama Y, Goda N, Kanai M, Niwa D, Osanai K, Yamamoto Y, et al. HIF-1alpha induction suppresses excessive lipid accumulation in alcoholic fatty liver in mice. J Hepatol. 2012;56(2):441-7.10.1016/j.jhep.2011.07.024

19.   Ni Q, Shao Y, Wang YZ, Jing YH, Zhang YC. Impact of high altitude on the hepatic fatty acid oxidation and synthesis in rats. Biochemical and Biophysical Research Communications. 2014;446(2):574-9.https://doi.org/10.1016/j.bbrc.2014.03.001

20.   Koh MY, Powis G. Passing the baton: the HIF switch. Trends Biochem Sci. 2012;37(9):364-72.10.1016/j.tibs.2012.06.004

21.   Broom AJ, Ambroso J, Brunori G, Burns AK, Armitage JR, Francis I, et al. Effects of mid-respiratory chain inhibition on mitochondrial function in vitro and in vivo. Toxicology Research. 2016;5(1):136-50

22.   Horscroft JA, Burgess SL, Hu Y, Murray AJ. Altered Oxygen Utilisation in Rat Left Ventricle and Soleus after 14 Days, but Not 2 Days, of Environmental Hypoxia. PLOS ONE. 2015;10(9):e0138564.10.1371/journal.pone.0138564

23.   Capper MJ, O'Neill PM, Fisher N, Strange RW, Moss D, Ward SA, et al. Antimalarial 4(1H)-pyridones bind to the Qi site of cytochrome bc1. Proceedings of the National Academy of Sciences. 2015;112(3):755-60.10.1073/pnas.1416611112

24.   Sotocina SG, Sorge RE, Zaloum A, Tuttle AH, Martin LJ, Wieskopf JS, et al. The Rat Grimace Scale: A Partially Automated Method for Quantifying Pain in the Laboratory Rat via Facial Expressions. Molecular Pain. 2011;7:1744-8069-7-55.10.1186/1744-8069-7-55

25.   Kamimura S, Gaal K, Britton RS, Bacon BR, Triadafilopoulos G, Tsukamoto H. Increased 4-hydroxynonenal levels in experimental alcoholic liver disease: Association of lipid peroxidation with liver fibrogenesis. Hepatology. 1992;16(2):448-53.10.1002/hep.1840160225

26.   Mata JM, Kershenobich D, Villarreal E, Rojkind M. Serum Free Proline and Free Hydroxyproline in Patients with Chronic Liver Disease. Gastroenterology. 1975;68(5):1265-9.10.1016/S0016-5085(75)80243-5

27.   Ducluzeau P-H, Lachaux A, Bouvier R, Streichenberger N, Stepien G, Mousson B. Depletion of mitochondrial DNA associated with infantile cholestasis and progressive liver fibrosis. Journal of Hepatology. 1999;30(1):149-55.https://doi.org/10.1016/S0168-8278(99)80019-1

28.   Carr A, Morey A, Mallon P, Williams D, Thorburn DR. Fatal portal hypertension, liver failure, and mitochondrial dysfunction after HIV-1 nucleoside analogue-induced hepatitis and lactic acidaemia. The Lancet. 2001;357(9266):1412-4.https://doi.org/10.1016/S0140-6736(00)04579-7

29.   Savolainen E-R, Leo MA, Timpl R, Lieber CS. Acetaldehyde and lactate stimulate collagen synthesis of cultured baboon liver myofibroblasts. Gastroenterology. 1984;87(4):777-87.10.1016/0016-5085(84)90070-2

30.   Larsen S, Nielsen J, Hansen CN, Nielsen LB, Wibrand F, Stride N, et al. Biomarkers of mitochondrial content in skeletal muscle of healthy young human subjects. The Journal of Physiology. 2012;590(14):3349-60.10.1113/jphysiol.2012.230185

31.   Jha P, Wang X, Auwerx J. Analysis of Mitochondrial Respiratory Chain Supercomplexes Using Blue Native Polyacrylamide Gel Electrophoresis (BN-PAGE). Current Protocols in Mouse Biology. 2016;6(1):1-14.doi:10.1002/9780470942390.mo150182

32.   Greggio C, Jha P, Kulkarni SS, Lagarrigue S, Broskey NT, Boutant M, et al. Enhanced Respiratory Chain Supercomplex Formation in Response to Exercise in Human Skeletal Muscle. Cell Metabolism. 2017;25(2):301-11.https://doi.org/10.1016/j.cmet.2016.11.004

33.   Zhang M, Mileykovskaya E, Dowhan W. Gluing the respiratory chain together. Cardiolipin is required for supercomplex formation in the inner mitochondrial membrane. The Journal of biological chemistry. 2002;277(46):43553-6.10.1074/jbc.C200551200

34.   Osman C, Voelker DR, Langer T. Making heads or tails of phospholipids in mitochondria. The Journal of Cell Biology. 2011;192(1):7-16.10.1083/jcb.201006159

35.   Schlame M, Haldar D. Cardiolipin is synthesized on the matrix side of the inner membrane in rat liver mitochondria. Journal of Biological Chemistry. 1993;268(1):74-9

36.   Schlame M, Horvàth L, Vìgh L. Relationship between lipid saturation and lipid-protein interaction in liver mitochondria modified by catalytic hydrogenation with reference to cardiolipin molecular species. Biochemical Journal. 1990;265(1):79-85.10.1042/bj2650079

37.   Cogliati S, Calvo E, Loureiro M, Guaras AM, Nieto-Arellano R, Garcia-Poyatos C, et al. Mechanism of super-assembly of respiratory complexes III and IV. Nature. 2016;539(7630):579-82.10.1038/nature20157

38.   Cogliati S, Frezza C, Soriano Maria E, Varanita T, Quintana-Cabrera R, Corrado M, et al. Mitochondrial Cristae Shape Determines Respiratory Chain Supercomplexes Assembly and Respiratory Efficiency. Cell. 2013;155(1):160-71.https://doi.org/10.1016/j.cell.2013.08.032

39.   Patten DA, Wong J, Khacho M, Soubannier V, Mailloux RJ, Pilon-Larose K, et al. OPA1-dependent cristae modulation is essential for cellular adaptation to metabolic demand. The EMBO Journal. 2014;33(22):2676-91.10.15252/embj.201488349

40.   An H-J, Cho G, Lee J-O, Paik S-G, Kim YS, Lee H. Higd-1a interacts with Opa1 and is required for the morphological and functional integrity of mitochondria. Proceedings of the National Academy of Sciences. 2013;110(32):13014-9.10.1073/pnas.1307170110

41.   Mitsopoulos P, Chang Y-H, Wai T, König T, Dunn SD, Langer T, et al. Stomatin-Like Protein 2 Is Required for In Vivo Mitochondrial Respiratory Chain Supercomplex Formation and Optimal Cell Function. Molecular and Cellular Biology. 2015;35(10):1838-47.10.1128/mcb.00047-15

42.   Semenza GL, Roth PH, Fang HM, Wang GL. Transcriptional regulation of genes encoding glycolytic enzymes by hypoxia-inducible factor 1. Journal of Biological Chemistry. 1994;269(38):23757-63

43.   Anundi I, Groot Hd. Hypoxic liver cell death: critical Po2 and dependence of viability on glycolysis. American Journal of Physiology-Gastrointestinal and Liver Physiology. 1989;257(1):G58-G64.10.1152/ajpgi.1989.257.1.G58

44.   Sanders FWB, Acharjee A, Walker C, Marney L, Roberts LD, Imamura F, et al. Hepatic steatosis risk is partly driven by increased de novo lipogenesis following carbohydrate consumption. Genome Biology. 2018;19(1):79.10.1186/s13059-018-1439-8

45.   Horscroft JA, Kotwica AO, Laner V, West JA, Hennis PJ, Levett DZH, et al. Metabolic basis to Sherpa altitude adaptation. Proceedings of the National Academy of Sciences. 2017;114(24):6382.10.1073/pnas.1700527114

46.   Bruder ED, Raff H. Cardiac and plasma lipid profiles in response to acute hypoxia in neonatal and young adult rats. Lipids Health Dis. 2010;9:3.10.1186/1476-511x-9-3

47.   Heathers GP, Yamada KA, Kanter EM, Corr PB. Long-chain acylcarnitines mediate the hypoxia-induced increase in alpha 1-adrenergic receptors on adult canine myocytes. Circulation research. 1987;61(5):735-46.10.1161/01.res.61.5.735

48.   McHowat J, Yamada KA, Saffitz JE, Corr PB. Subcellular distribution of endogenous long chain acylcarnitines during hypoxia in adult canine myocytes. Cardiovasc Res. 1993;27(7):1237-43.10.1093/cvr/27.7.1237

49.   Kennedy SL, Stanley WC, Panchal AR, Mazzeo RS. Alterations in enzymes involved in fat metabolism after acute and chronic altitude exposure. Journal of applied physiology (Bethesda, Md : 1985). 2001;90(1):17-22.10.1152/jappl.2001.90.1.17

50.   Kinnula VL, Hassinen I. Effect of chronic hypoxia on hepatic triacylglycerol concentration and mitochondrial fatty acid oxidizing capacity in liver and heart. Acta Physiologica Scandinavica. 1978;102(1):64-73.https://doi.org/10.1111/j.1748-1716.1978.tb06046.x

51.   Koves TR, Ussher JR, Noland RC, Slentz D, Mosedale M, Ilkayeva O. Mitochondrial overload and incomplete fatty acid oxidation contribute to skeletal muscle insulin resistance. Cell Metab. 2008;7.10.1016/j.cmet.2007.10.013

52.   Patterson RE, Kalavalapalli S, Williams CM, Nautiyal M, Mathew JT, Martinez J, et al. Lipotoxicity in steatohepatitis occurs despite an increase in tricarboxylic acid cycle activity. American Journal of Physiology-Endocrinology and Metabolism. 2016;310(7):E484-E94.10.1152/ajpendo.00492.2015

1003   53.   Bruss MD, Khambatta CF, Ruby MA, Aggarwal I, Hellerstein MK. Calorie restriction increases
1004 fatty acid synthesis and whole body fat oxidation rates. American Journal of Physiology-
1005 Endocrinology and Metabolism. 2010;298(1):E108-E16.10.1152/ajpendo.00524.2009
1006   54.   Montagner A, Polizzi A, Fouché E, Ducheix S, Lippi Y, Lasserre F, et al. Liver PPARα is crucial
1007 for whole-body fatty acid homeostasis and is protective against NAFLD. Gut. 2016;65(7):1202-
1008 14.10.1136/gutjnl-2015-310798
1009   55.   Cerqueira FM, Cunha FM, Laurindo FRM, Kowaltowski AJ. Calorie restriction increases
1010 cerebral mitochondrial respiratory capacity in a NO•-mediated mechanism: Impact on neuronal
1011 survival. Free Radical Biology and Medicine. 2012;52(7):1236-
1012 41.https://doi.org/10.1016/j.freeradbiomed.2012.01.011
1013   56.   Marchetti P, Fovez Q, Germain N, Khamari R, Kluza J. Mitochondrial spare respiratory
1014 capacity: Mechanisms, regulation, and significance in non-transformed and cancer cells. The FASEB
1015 Journal. 2020;34(10):13106-24.https://doi.org/10.1096/fj.202000767R
1016   57.   Semenza GL, Wang GL. A nuclear factor induced by hypoxia via de novo protein synthesis
1017 binds to the human erythropoietin gene enhancer at a site required for transcriptional activation.
1018 Molecular and Cellular Biology. 1992;12(12):5447-54.10.1128/mcb.12.12.5447
1019   58.   Lapuente-Brun E, Moreno-Loshuertos R, Acín-Pérez R, Latorre-Pellicer A, Colás C, Balsa E, et
1020 al. Supercomplex Assembly Determines Electron Flux in the Mitochondrial Electron Transport Chain.
1021 Science. 2013;340(6140):1567-70.10.1126/science.1230381
1022   59.   Acin-Perez R, Enriquez JA. The function of the respiratory supercomplexes: The plasticity
1023 model. Biochimica et Biophysica Acta (BBA) - Bioenergetics. 2014;1837(4):444-
1024 50.https://doi.org/10.1016/j.bbabio.2013.12.009
1025   60.   Antoun G, McMurray F, Thrush AB, Patten DA, Peixoto AC, Slack RS, et al. Impaired
1026 mitochondrial oxidative phosphorylation and supercomplex assembly in rectus abdominis muscle of
1027 diabetic obese individuals. Diabetologia. 2015;58(12):2861-6.10.1007/s00125-015-3772-8
1028   61.   Hollinshead KER, Parker SJ, Eapen VV, Encarnacion-Rosado J, Sohn A, Oncu T, et al.
1029 Respiratory Supercomplexes Promote Mitochondrial Efficiency and Growth in Severely Hypoxic
1030 Pancreatic Cancer. Cell Reports. 2020;33(1):108231.https://doi.org/10.1016/j.celrep.2020.108231
1031   62.   Denko N, Schindler C, Koong A, Laderoute K, Green C, Giaccia A. Epigenetic Regulation of
1032 Gene Expression in Cervical Cancer Cells by the Tumor Microenvironment. Clinical Cancer Research.
1033 2000;6(2):480-7
1034   63.   An H-J, Shin H, Jo S-G, Kim YJ, Lee J-O, Paik S-G, et al. The survival effect of mitochondrial
1035 Higd-1a is associated with suppression of cytochrome C release and prevention of caspase
1036 activation. Biochimica et Biophysica Acta (BBA) - Molecular Cell Research. 2011;1813(12):2088-
1037 98.https://doi.org/10.1016/j.bbamcr.2011.07.017
1038   64.   Zhang X, Degenstein L, Cao Y, Stein J, Osei K, Wang J. β-Cells with Relative Low HIMP1
1039 Overexpression Levels in a Transgenic Mouse Line Enhance Basal Insulin Production and
1040 Hypoxia/Hypoglycemia Tolerance. PLOS ONE. 2012;7(3):e34126.10.1371/journal.pone.0034126
1041   65.   Hayashi T, Asano Y, Shintani Y, Aoyama H, Kioka H, Tsukamoto O, et al. Higd1a is a positive
1042 regulator of cytochrome c oxidase. Proceedings of the National Academy of Sciences.
1043 2015;112(5):1553-8.10.1073/pnas.1419767112
1044   66.   Timón-Gómez A, Garlich J, Stuart RA, Ugalde C, Barrientos A. Distinct Roles of Mitochondrial
1045 HIGD1A and HIGD2A in Respiratory Complex and Supercomplex Biogenesis. Cell Reports.
1046 2020;31(5):107607.https://doi.org/10.1016/j.celrep.2020.107607
1047   67.   Charidemou E, Ashmore T, Li X, McNally BD, West JA, Liggi S, et al. A randomized 3-way
1048 crossover study indicates that high-protein feeding induces de novo lipogenesis in healthy humans.
1049 JCI Insight. 2019;4(12):e124819.10.1172/jci.insight.124819
1050   68.   Coleman RA, Lee DP. Enzymes of triacylglycerol synthesis and their regulation. Progress in
1051 Lipid Research. 2004;43(2):134-76.https://doi.org/10.1016/S0163-7827(03)00051-1
1052   69.   Sanders FWB, Griffin JL. De novo lipogenesis in the liver in health and disease: more than
1053 just a shunting yard for glucose. Biological Reviews. 2016;91(2):452-68.10.1111/brv.12178

39

1054 70.	Foster DW, Bloom B. The synthesis of fatty acids by rat liver slices in tritiated water. . Journal
1055 of Biological Chemistry (US). 1963:Medium: X; Size: Pages: 888-92

1056 71.	Hellerstein MK, Christiansen M, Kaempfer S, Kletke C, Wu K, Reid JS, et al. Measurement of
1057 de novo hepatic lipogenesis in humans using stable isotopes. The Journal of clinical investigation.
1058 1991;87(5):1841-52.10.1172/JCI115206

1059 72.	Guillou H, Zadravec D, Martin PGP, Jacobsson A. The key roles of elongases and desaturases
1060 in mammalian fatty acid metabolism: Insights from transgenic mice. Progress in Lipid Research.
1061 2010;49(2):186-99.https://doi.org/10.1016/j.plipres.2009.12.002

1062 73.	Kamphorst JJ, Cross JR, Fan J, de Stanchina E, Mathew R, White EP, et al. Hypoxic and Ras-
1063 transformed cells support growth by scavenging unsaturated fatty acids from lysophospholipids.
1064 Proceedings of the National Academy of Sciences. 2013;110(22):8882-7.10.1073/pnas.1307237110

1065 74.	Charidemou E, Ashmore T, Li X, McNally BD, West JA, Liggi S, et al. A randomized 3-way
1066 crossover study indicates that high-protein feeding induces de novo lipogenesis in healthy humans.
1067 JCI Insight. 2019;4(12).10.1172/jci.insight.124819

1068 75.	Schwarz JM, Neese RA, Turner S, Dare D, Hellerstein MK. Short-term alterations in
1069 carbohydrate energy intake in humans. Striking effects on hepatic glucose production, de novo
1070 lipogenesis, lipolysis, and whole-body fuel selection. The Journal of Clinical Investigation.
1071 1995;96(6):2735-43.10.1172/JCI118342

1072 76.	Pasarica M, Rood J, Ravussin E, Schwarz J-M, Smith SR, Redman LM. Reduced Oxygenation in
1073 Human Obese Adipose Tissue Is Associated with Impaired Insulin Suppression of Lipolysis. The
1074 Journal of Clinical Endocrinology & Metabolism. 2010;95(8):4052-5.10.1210/jc.2009-2377

1075 77.	García-Fuentes E, Santiago-Fernández C, Gutiérrez-Repiso C, Mayas MD, Oliva-Olivera W,
1076 Coín-Aragüez L, et al. Hypoxia is associated with a lower expression of genes involved in lipogenesis
1077 in visceral adipose tissue. Journal of Translational Medicine. 2015;13(1):373.10.1186/s12967-015-
1078 0732-5

1079 78.	Mahat B, Chassé É, Mauger J-F, Imbeault P. Effects of acute hypoxia on human adipose
1080 tissue lipoprotein lipase activity and lipolysis. Journal of Translational Medicine.
1081 2016;14(1):212.10.1186/s12967-016-0965-y

1082 79.	Raclot T, Mioskowski E, Bach AC, Groscolas R. Selectivity of fatty acid mobilization: a general
1083 metabolic feature of adipose tissue. American Journal of Physiology-Regulatory, Integrative and
1084 Comparative Physiology. 1995;269(5):R1060-R7.10.1152/ajpregu.1995.269.5.R1060

1085 80.	Raclot T. Selective mobilization of fatty acids from adipose tissue triacylglycerols. Progress in
1086 lipid research. 2003;42(4):257-88.10.1016/s0163-7827(02)00066-8

1087 81.	Mantena Sudheer K, Vaughn Denty P, Jr, Andringa Kelly K, Eccleston Heather B, King
1088 Adrienne L, Abrams Gary A, et al. High fat diet induces dysregulation of hepatic oxygen gradients and
1089 mitochondrial function in vivo. Biochemical Journal. 2008;417(1):183-93.10.1042/bj20080868

1090 82.	Savransky V, Bevans S, Nanayakkara A, Li J, Smith PL, Torbenson MS, et al. Chronic
1091 intermittent hypoxia causes hepatitis in a mouse model of diet-induced fatty liver. American Journal
1092 of Physiology-Gastrointestinal and Liver Physiology. 2007;293(4):G871-G7.10.1152/ajpgi.00145.2007

1093 83.	Chen X, Li L, Liu X, Luo R, Liao G, Li L, et al. Oleic acid protects saturated fatty acid mediated
1094 lipotoxicity in hepatocytes and rat of non-alcoholic steatohepatitis. Life Sciences. 2018;203:291-
1095 304.https://doi.org/10.1016/j.lfs.2018.04.022

1096 84.	McKenna HT, O'Brien KA, Fernandez BO, Minnion M, Tod A, McNally BD, et al. Divergent
1097 trajectories of cellular bioenergetics, intermediary metabolism and systemic redox status in survivors
1098 and non-survivors of critical illness. Redox Biology.
1099 2021;41:101907.https://doi.org/10.1016/j.redox.2021.101907

1100 85.	Sowton AP, Padmanabhan N, Tunster SJ, McNally BD, Murgia A, Yusuf A, et al. Mtrr
1101 hypomorphic mutation alters liver morphology, metabolism and fuel storage in mice. Molecular
1102 Genetics and Metabolism Reports. 2020;23:100580.https://doi.org/10.1016/j.ymgmr.2020.100580

1103 86.	O'Brien KA, Horscroft JA, Devaux J, Lindsay RT, Steel AS, Clark AD, et al. PPARα-independent
1104 effects of nitrate supplementation on skeletal muscle metabolism in hypoxia. Biochimica et

Biophysica Acta (BBA) - Molecular Basis of Disease. 2019;1865(4):844-53.https://doi.org/10.1016/j.bbadis.2018.07.027

87.   West JA, Beqqali A, Ament Z, Elliott P, Pinto YM, Arbustini E, et al. A targeted metabolomics assay for cardiac metabolism and demonstration using a mouse model of dilated cardiomyopathy. Metabolomics. 2016;12(3):59.10.1007/s11306-016-0956-2

88.   Murgia A, Hinz C, Liggi S, Denes J, Hall Z, West J, et al. Italian cohort of patients affected by inflammatory bowel disease is characterised by variation in glycerophospholipid, free fatty acids and amino acid levels. Metabolomics. 2018;14(10):140.10.1007/s11306-018-1439-4

89.   Cajka T, Fiehn O. Increasing lipidomic coverage by selecting optimal mobile-phase modifiers in LC–MS of blood plasma. Metabolomics. 2016;12(2):34.10.1007/s11306-015-0929-x

90.   Fahy E, Sud M, Cotter D, Subramaniam S. LIPID MAPS online tools for lipid research. Nucleic Acids Research. 2007;35(suppl_2):W606-W12.10.1093/nar/gkm324

91.   Murphy RC, Axelsen PH. Mass spectrometric analysis of long-chain lipids. Mass Spectrometry Reviews. 2011;30(4):579-99.10.1002/mas.20284

92.   Schneider CA, Rasband WS, Eliceiri KW. NIH Image to ImageJ: 25 years of image analysis. Nature Methods. 2012;9(7):671-5.10.1038/nmeth.2089

93.   Yung HW, Colleoni F, Dommett E, Cindrova-Davies T, Kingdom J, Murray AJ, et al. Noncanonical mitochondrial unfolded protein response impairs placental oxidative phosphorylation in early-onset preeclampsia. Proceedings of the National Academy of Sciences. 2019;116(36):18109-18.10.1073/pnas.1907548116

94.   Chong J, Soufan O, Li C, Caraus I, Li S, Bourque G, et al. MetaboAnalyst 4.0: towards more transparent and integrative metabolomics analysis. Nucleic acids research. 2018;46(W1):W486-w94.10.1093/nar/gky310

95.   O'Brien KA, McNally MB, Sowton AP, Murgia A, Armitage J, Thomas LW, Krause FN, Maddalena LA, Francis I, Kavanagh S, Williams DP, Ashcroft M, Griffin JL, Lyon JJ, Murray AJ. . Data supporting "Enhanced hepatic respiratory capacity and altered lipid metabolism support metabolic homeostasis during short-term hypoxic stress". Cambridge University Repository. 2021.https://doi.org/10.17863/CAM.75680

96.   Haug K, Cochrane K, Nainala VC, Williams M, Chang J, Jayaseelan KV, et al. MetaboLights: a resource evolving in response to the needs of its scientific community. Nucleic acids research. 2020;48(D1):D440-d4.10.1093/nar/gkz1019

97.   O'Brien KA, McNally MB, Sowton AP, Murgia A, Armitage J, Thomas LW, Krause FN, Maddalena LA, Francis I, Kavanagh S, Williams DP, Ashcroft M, Griffin JL, Lyon JJ, Murray AJ. Metabolomics data supporting "Enhanced hepatic respiratory capacity and altered lipid metabolism support metabolic homeostasis during short-term hypoxic stress". EMBL-EBI Metabolights. 2021.https://www.ebi.ac.uk/metabolights/MTBLS3713
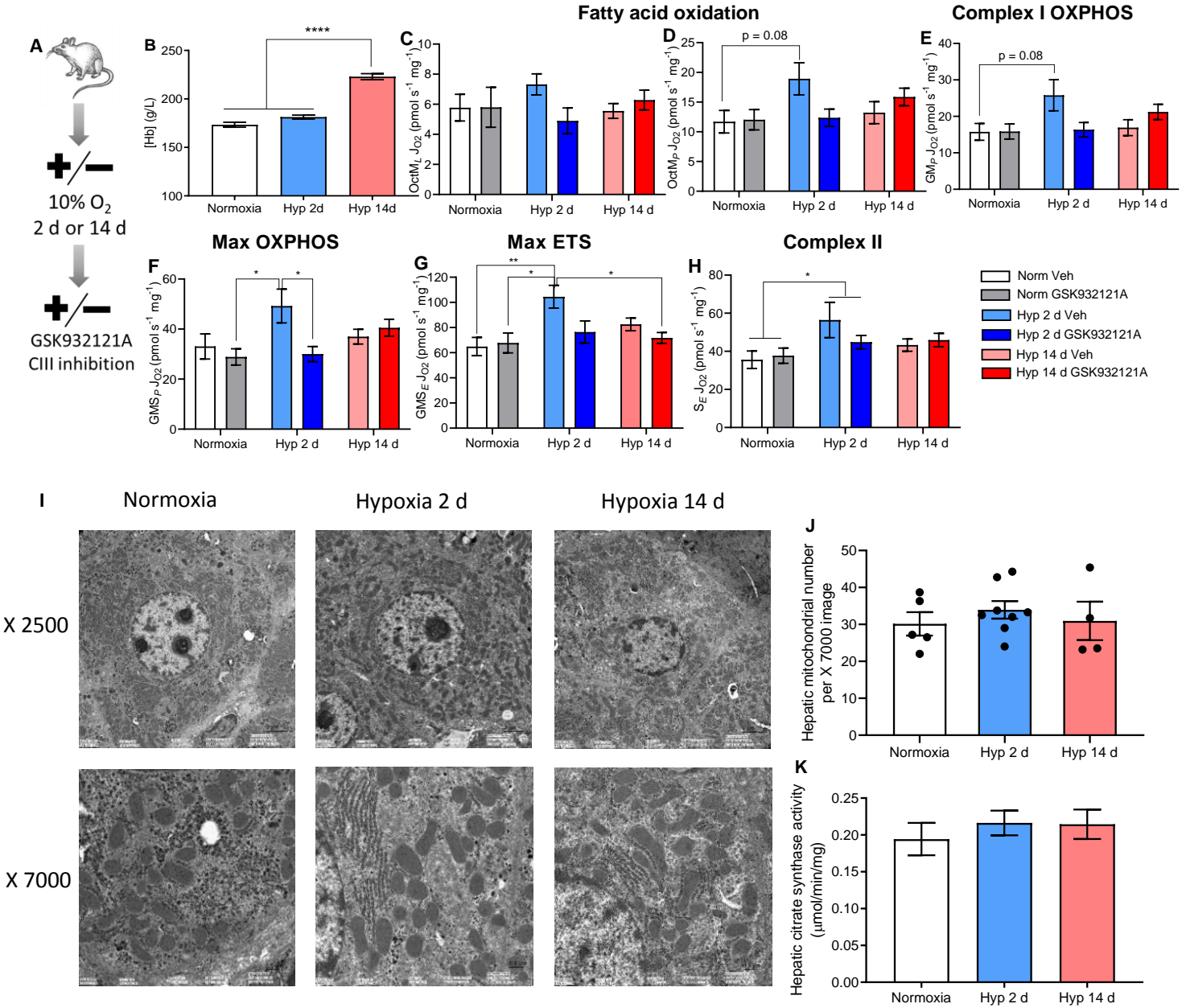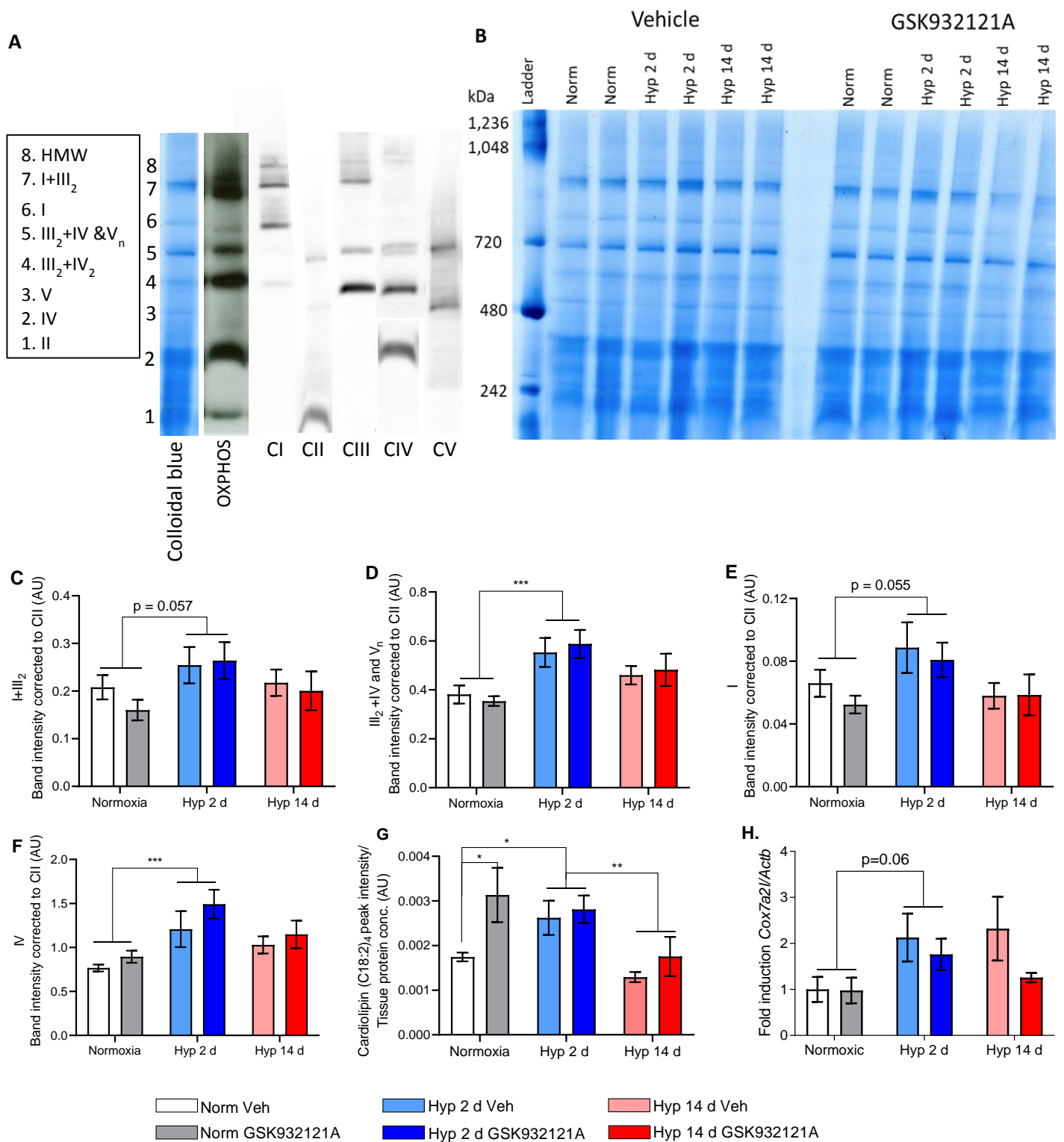
Figure 1

Figure 2

Figure 3

Figure 4
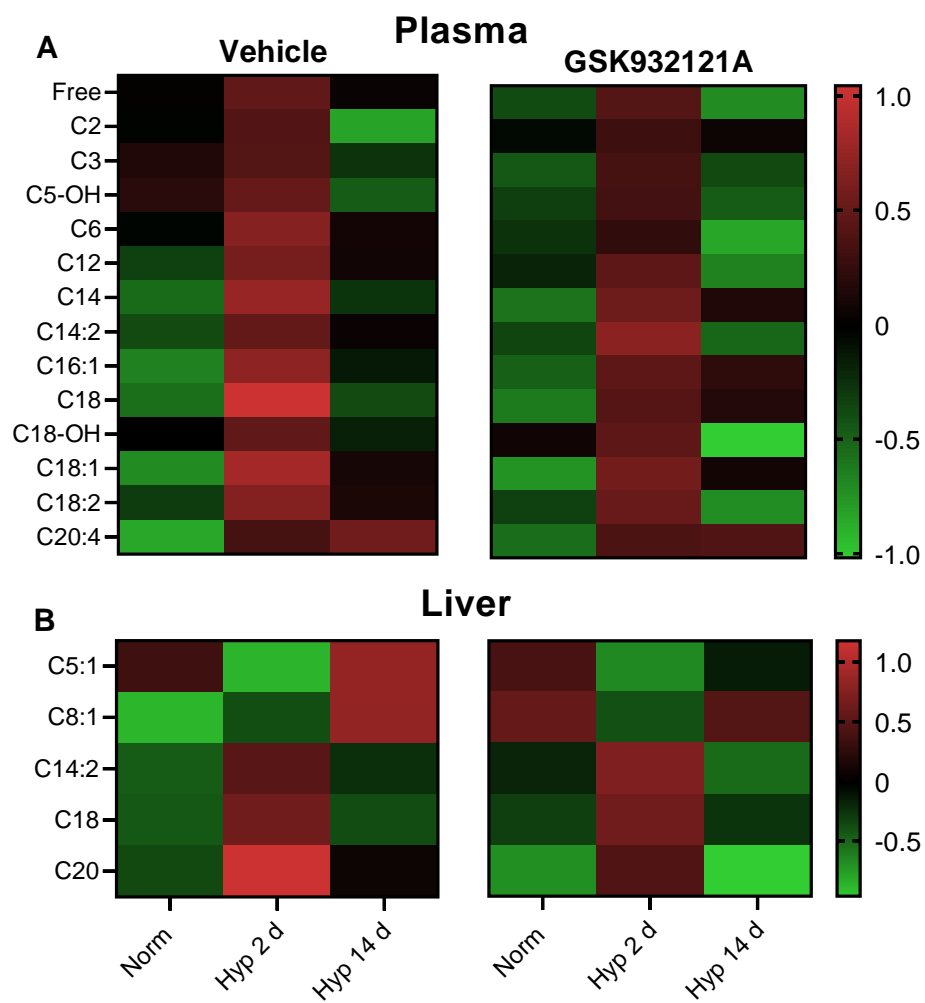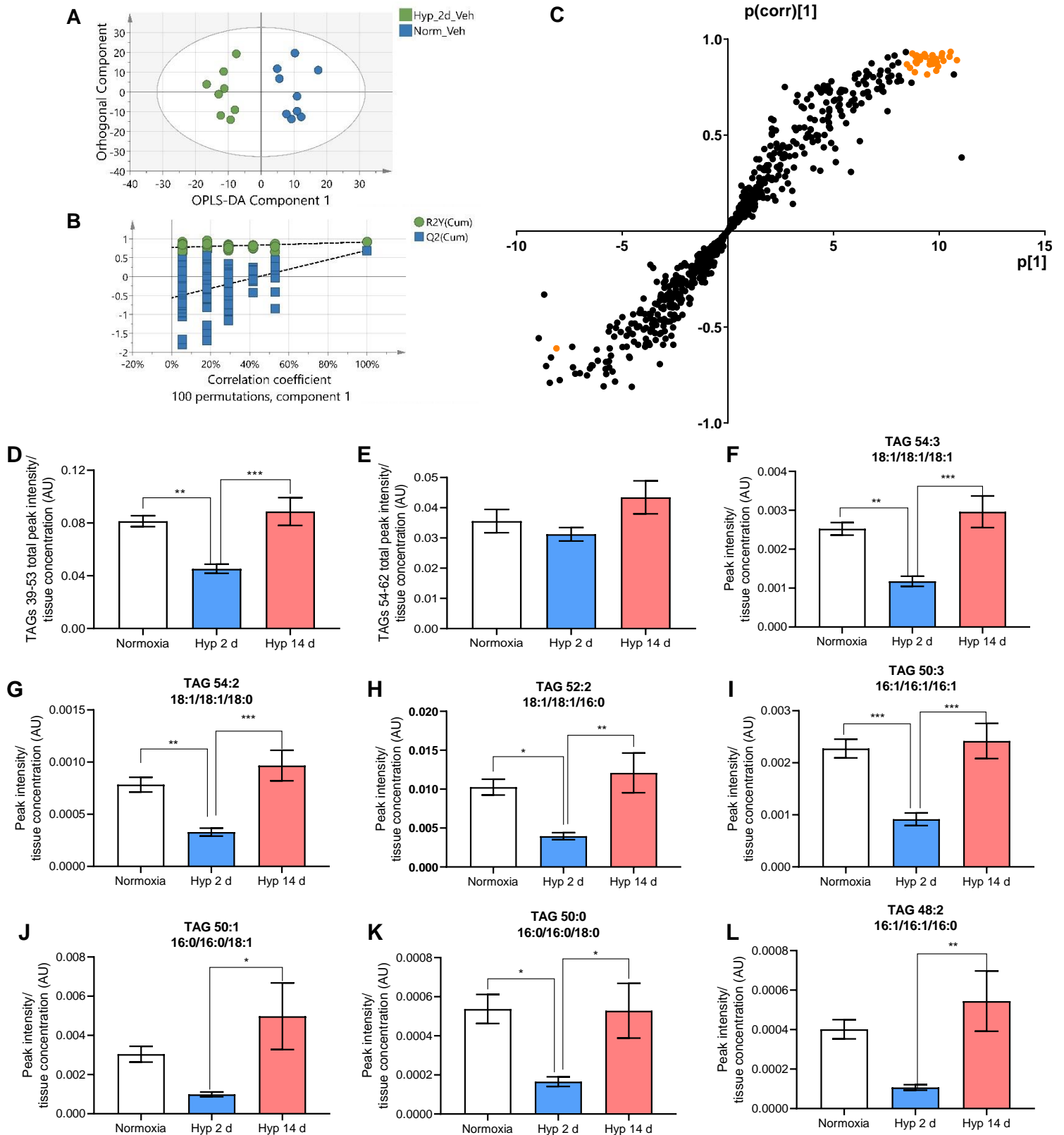

A Plasma

Vehicle | GSK932121A

Figure 5

Dr Katie O'Brien
Marie Sklodowska-Curie Global Fellow

UNIVERSITY OF CAMBRIDGE

Department of Physiology, Development & Neuroscience

11th November 2021

Dear Dr Bell

Manuscript Number: BMCB-D-21-00115R3

My co-authors and I would again like to express our thanks to you, your team and the Reviewers for the time taken over our manuscript. We are delighted that our work has been accepted for publication.

Please find attached a revised version of our manuscript with the titled: *Enhanced hepatic respiratory capacity and altered lipid metabolism support metabolic homeostasis during short-term hypoxic stress*.

We have addressed the points you raised. The Change of Authorship form and confirmation from all authors have been sent via email. The raw mass spectrometry data has been deposited to the EMBL-EBI MetaboLights database with the identifier MTBLS3713. This information has been included in the 'Availability of Data' section of the manuscript.

We very much hope that you find our alterations to the manuscript satisfactory and that our work is now ready for publication in BMC Biology.

Yours Sincerely

Dr Katie O'Brien

University of Cambridge,
Department of Physiology, Development & Neuroscience,
Physiological Laboratory,
Downing Street,
Cambridge, CB2 3EG.

Telephone: 01223 766789
E-mail: ko337@cam.ac.uk

Click here to access/download
Supplementary Material
Additional File 1 Supplementary Figs.docx